JOURNAL OF QUATERNARY SCIENCE (2020) **35**(1-2) 213–231 ISSN 0267-8179. DOI: 10.1002/jqs.3154

JQS Journal of Quaternary Science QRA Quaternary Research Association

The Late Holocene tephra record of the central Mediterranean Sea: Mapping occurrences and new potential isochrons for the 4.4–2.0 ka time interval

D. D. INSINGA,[1]* P. PETROSINO,[2] I. ALBERICO,[1] G. J. DE LANGE,[3] C. LUBRITTO,[4] F. MOLISSO,[1] M. SACCHI,[1] R. SULPIZIO,[5] J. WU[3,6] and F. LIRER[1]

[1]Istituto di Scienze Marine (ISMAR), CNR, Calata Porta di Massa, Interno Porto di Napoli, Napoli, Italy
[2]Dipartimento di Scienze della Terra dell'Ambiente e delle Risorse (DiSTAR), Università degli Studi 'Federico II' di Napoli, Italy
[3]Department of Earth Sciences-Geochemistry, Utrecht University, The Netherlands
[4]Dipartimento di Scienze e Tecnologie Ambientali, Biologiche e Farmaceutiche, Università della Campania 'Luigi Vanvitelli', Caserta, Italy
[5]Dipartimento di Scienze della Terra e Geoambientali, Università di Bari, Italy
[6]State Key Laboratory of Marine Geology, Tongji University, China

Received 28 March 2019; Revised 2 October 2019; Accepted 7 October 2019

ABSTRACT: Five cores from the southern Tyrrhenian and Ionian seas were studied for their tephra and cryptotephra content in the 4.4–2.0 ka time interval. The chronological framework for each core was obtained by accelerator mass spectrometry ^{14}C dating, the occurrence of distinct marker tephra and stratigraphic correlation with adjacent records. Tephrochronology allowed us to correlate the analyzed deposits with tephra markers associated with Somma-Vesuvius (79 AD), Ischia Island (Cretaio), Mt Etna (FG, FL and FS) and Campi Flegrei (Astroni-Agnano Monte Spina) events. For the first time in the marine setting, a large single glass data set is provided for the Late Holocene Etnean marker beds including the FS tephra (ca. 4.3 ka). Moreover, unknown deposits from Lipari (ca. 2.2–2.0 ka) and Vulcano (3.6–3.3 ka) are also recognized at more distal sites than previously reported. These results contribute to improve the high-resolution tephrostratigraphic framework of the central Mediterranean Sea. They also provide new insights into the chemical composition and dispersal pattern of tephras that can be used as inter-archive tools for regional and 'local' stratigraphic correlations and for addressing paleoclimate research.
Copyright © 2019 John Wiley & Sons, Ltd.

KEYWORDS: central Mediterranean; cryptotephra; isochronous marker; Italian volcanism; tephra.

Introduction

The need for high-resolution, robust chronostratigraphic records, mainly for paleoclimate research, has resulted in numerous tephra and cryptotephra studies over the last decade (e.g. Abbott *et al.*, 2018). This is particularly true for the central Mediterranean, a key area for tephrochronology due to the occurrence of active volcanoes during the Quaternary and the availability of long and continuous marine and continental archives (e.g. Keller *et al.*, 1978; Paterne *et al.*, 1988, 2008; Calanchi *et al.*, 1998; Siani *et al.*, 2004; Wulf *et al.*, 2004; Munno and Petrosino, 2007; Sulpizio *et al.*, 2010; Insinga *et al.*, 2014; Matthews *et al.*, 2015; Giaccio *et al.*, 2017). To date, in the marine setting, tephra and cryptotephra have been analyzed in ca. 129 sediment cores (198 in the whole Mediterranean) (Alberico *et al.*, 2017). As a result, more refined tephrostratigraphic frameworks for the Late Quaternary are now available from shelf to basin. They include mostly major tephra markers related to high-energy volcanic events (e.g. Wulf *et al.*, 2008; Zanchetta *et al.*, 2011; Bronk Ramsey *et al.*, 2015; Tomlinson *et al.*, 2015) and, to a lesser extent, deposits from moderately explosive eruptions (Sacchi *et al.*, 2009; Lirer *et al.*, 2013; Crocitti *et al.*, 2018; Di Donato *et al.*, 2019). These studies have relied heavily on recent advancements in the methods and technology of sampling systems, that allow for the recovery of undisturbed sediment cores with the possibility of retrieving tephra and cryptotephra deposited in recent centuries even in the few centimeters of the sub-sea floor (e.g. Jalali *et al.*, 2018; Margaritelli et al., 2016). Improved results in terms of tephra correlation have also been derived from high-precision characterization of glass composition at proximal sites. A large database compiled in recent years for Somma-Vesuvius and Campi Flegrei volcanoes (Santacroce *et al.*, 2008; Smith *et al.*, 2011; Tomlinson *et al.*, 2012), for example, has provided a significant contribution to the recognition of distal tephra and associated source vents. Conversely, for other eruptive centers, such as the Aeolian Islands and Mt Etna, chemistry from single glass shards is available only for major markers (Albert *et al.*, 2012, 2013, 2017). As a result, a number of distal deposits, found in both the Tyrrhenian and the Ionian seas and related to moderately explosive eruptions, are still uncorrelated (e.g. Paterne *et al.*, 1988; Di Donato *et al.*, 2019).

In this study we present a tephrostratigraphic framework for the 4.4–2.0 ka time interval of the central Mediterranean underpinned by the analysis of five marine cores. Our results are integrated with the Weather and Water Database (WDB)-Paleo, which records paleoproxy metadata from the extensive marine core network (Alberico *et al.*, 2017). The main outcomes of this work include the detection of tephra with 'local' correlation potential and the definition of robust isochrons for high-resolution stratigraphy.

*Correspondence: D. D. Insinga, as above.
E-mail: donatelladomenica.insinga@cnr.it

Copyright © 2019 John Wiley & Sons, Ltd.

Data set and analytical methods

Gravity cores

The tephra and cryptotephra analyzed in this work were sampled from cores located in the southern Tyrrhenian and Ionian Seas (Fig. 1). They were collected between 1994 and 2012 in the framework of several research projects on board the Research Vessel (R/V) *Urania* of the Italian Research Council (cores C14, C1, AP1.1, UM42BC) and the RV *Pelagia* (core CP10BC). Details are reported in Table 1.

Southern Tyrrhenian Sea

Gravity core C14 was recovered during the GMS98-01 cruise dedicated to the geological mapping of continental and marine areas (CARG project, 1997–2004). A 5.22-m-long succession was retrieved from the western sector of Naples Bay at a depth of 186.5 m below sea level (bsl) and it is composed of silt deposits with volcaniclastic turbidites and interbedded primary tephra layers. The stratigraphic record sampled at the C14 site spans the last ca. 9 ka (Petrosino *et al.*, 2018).

Gravity core MSK-12 C1 (hereafter C1) was acquired during the MARISK_12 cruise along the eastern Tyrrhenian margin. The 4.50-m-long record is located offshore Capo Vaticano at a depth of 604 m below the sea floor (bsf) and it is mostly composed of silt and interbedded primary tephra deposited during the last 17 ka (our unpublished data).

Ionian Sea

Gravity core AP1.1 (hereafter AP1) was sampled in the northern Ionian Sea during Sin-Sap 98 cruise. The 3.20-m-long succession is located at 811 m bsl and characterized by silt deposits which include sapropels S1, S3 and S5 (D'Antonio *et al.*, 2016).

Box core UM42BC (hereafter UM42) was recovered in the western Ionian Sea at a depth of 1375 m bsl during the oceanographic cruise Urania 18. It is 35.5 cm long and

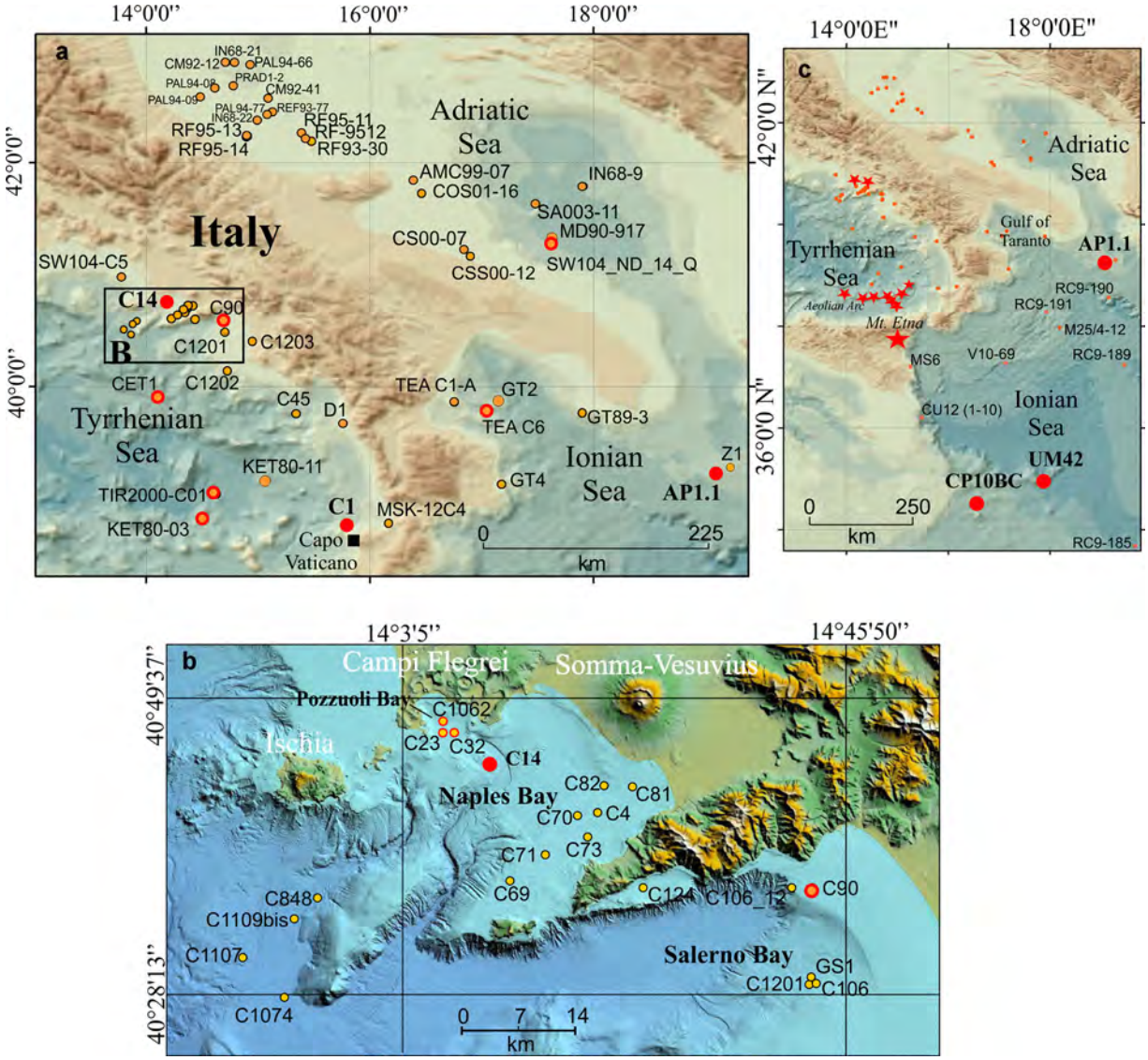

Figure 1. Location of the studied cores (red full circles). All cores containing tephra related to the studied time span in the investigated area have been selected from the WDB-Paleo database and are reported in the figure. Red (border) and orange (center) circles refer to cores cited in the text. Digital Terrain Model of the Naples Bay (inset B) courtesy of R. Tonielli. References: SW104-C5 in Margaritelli *et al.* (2016); C1201 and C1202 in Iorio *et al.* (2009); C1203 in Budillon *et al.* (2012); C106 and C45 in Munno and Petrosino (2004); CET 1 in Morabito *et al.* (2014); MSK-12C4 in Cosentino *et al.* (2017); TIR2000-C01 in Di Roberto *et al.* (2008); KET80-11 and 80-03 in Paterne *et al.* (1988); GS1, D1, GT2 and GT4 in Crocitti *et al.* (2018); TEA C1-A in Pepe *et al.* (2018); TEA C6 in Di Donato *et al.* (2019); GT89-3 in Cini Castagnoli *et al.* (1990); Z1 in Geraga *et al.* (2008); CU12 set in Micallef *et al.* (2016); MS6 in Smedile *et al.* (2011); SW104_ND_14Q in Jalali *et al.* (2018); cores RF-, PAL-, IN68- and CM- in Calanchi *et al.* (1998) and Calanchi and Dinelli (2008); CSS00-12, CSS00-07, COS01-16 and AMC99-07 in Lowe *et al.* (2007); core MD90-917 in Siani *et al.* (2004); cores in Naples and Pozzuoli bays in Sacchi *et al.* (2005, 2014); cores in the Ionian Sea in Keller *et al.* (1978). [Color figure can be viewed at wileyonlinelibrary.com]

Copyright © 2019 John Wiley & Sons, Ltd.

Table 1. Summary of core and tephra data presented in this work including source volcano and event.

Core	Location		Depth below sea level (m)	Length (m)	Age control along the record	Tephra-event (source)	*Type*/lithology	Composition	Age on proximal	Age in marine setting
C14	14°1130″ E	40°44′47″N	186.5	5.22	Stratigraphic relationship with other cores	C14/89-Pompei + Cretaio (SV + I)	*Visible tephra*/Light and light gray micropumice, dark scoria, lithics (some leucite bearing), loose crystals of feldspar and clinopyroxene.	Phonolite (population a) + Trachyphonolite (population b)	79 AD/1st century AD[1]	3 ± 42 AD for Cretaio[2]
C1	15°48.236′E	38°44.573′N	604	4.5	^{14}C and stratigraphic relationship with other cores	C1/56-Pompei (SV)	*Cryptotephra*/Light and light gray vesiculated micropumice, leucite-bearing lithics, loose crystals of feldspar and biotite	Phonolite	79 AD	–
						C1/82-FL (Et)	*Cryptotephra*/Dark to iron-gray porphyritic scoriaceous fragments, loose crystals and reddish lava lithic fragments	Benmoreite		
						C1/85–? (Vulc) + FL (Et)	*Cryptotephra*/Dark dense scoria and grayish pumice. Dark honey glass shards with blocky morphology also occur. Loose crystals of olivine, pyroxene and brown mica.	Mugearite (population a) + Tephriphonolite (SHO) (population b)	3361 ± 76 cal a BP (FL)[3]	
						C1/87-FL (Et)	*Cryptotephra*/Dark porphyritic scoria and grayish pumice. Loose crystals of feldspar and clinopyroxene	Benmoreite–trachyte		
						C1/90-FL (Et)	*Cryptotephra*/Dark gray porphyritic scoria	Benmoreite		3625 ± 96 cal a BP *(this study)*
SAPGCAP1.1	19°06.78′E	39°12.99′N	810	3.2	^{14}C datings, sedimentation rates	AP1/13*-FS + AAMS (Et + CF)	*Cryptotephra*/Dark gray dense scoria and rare pale gray pumice.	Benmoreite (population a) + Trachyphonolite (population b)	4.36 ± 0.092 cal ka BP[3]/4.6–4.1 cal ka BP[4]	4420 ± 60 cal a BP[5]; 4237 ± 44 cal a BP (*this study*)
UM42BC	17°51.75′E	34°57.23′N	1375	0.355	^{14}C datings, sedimentation rates	UM42/7*-FG (Et)	*Visible tephra*/Brown to yellowish vesiculated glass fragments with feldspar crystals and minor honey dense aphyric glass fragments. Dark brown and grayish	Mugearite to benmoreite	380 BC to 120 AD (122 BC historical age)[6]	~2.2 cal ka BP (*this study*)

(*Continued*)

Copyright © 2019 John Wiley & Sons, Ltd.

Table 1. (*Continued*)

Core	Location	Depth below sea level (m)	Length (m)	Age control along the record	Tephra-event (source)	*Type*/lithology	Composition	Age on proximal	Age in marine setting
						brown porphyritic scoria fragments, reddish lithics and loose crystals.			
CP10BC	16°34.00′E 34°32.70′N	1501	0.355	^{14}C datings, sedimentation rates	CP10BC/7*-FG + ? (Et + L)	*Cryptotephra*/Dark scoria, altered micropumice and few platy glass shards. Loose crystals of feldspar and brown mica	Mugearite–tephriphonolite (population a) + HKCA rhyolite (population b)	380 BC to 120 AD (122 BC historical age)[6]	1.97 cal ka BP for Lipari rhyolites[7] 2187 ± 37 cal a BP (*this study*)

Et: Etna, CF: Campi Flegrei, SV: Somma-Vesuvius, L: Lipari, Vulc: Vulcano. (1) Age for Cretaio from Orsi *et al.* (1992); (2) De Alteriis *et al.* (2010); (3) Coltelli *et al.* (2000); (4) Smith *et al.* (2011); (5) Lirer *et al.* (2013); (6) Coltelli *et al.* (1998); (7) Di Donato *et al.* (2019).
*Original sample code on board: AP1/13 = GG0128, UM42/7 = DD1320; CP10/7 = CP10BC#14.

represented by hemipelagites with interbedded sapropel S1 (Freydier *et al.*, 2001).

Box core CP10BC (hereafter CP10) was collected during the CORTADO-2011 cruise on the Lybian–Tunisian slope. It is 35.5 cm long and characterized by marly ooze with sapropel S1 as a distinct unit (Wu *et al.*, 2016, 2017).

Sampling and selection of materials

Two visible tephras and four cryptotephras were sampled and analyzed (Table 1). Where applicable (e.g. relatively thick deposits) or where required for specific purposes (e.g. ultrahigh-resolution stratigraphic studies), a number of subsamples were taken from the same deposit. All samples were labeled according to the identifying core code/name and depth (cm) below the sea floor.

Sediment samples were disaggregated in distilled water and wet sieved at 63, 90, 125 and 250 μm to remove the fine-grained fraction. The sieved material was cleaned with an ultrasonic probe and dried at 60 °C. A magnetic separator was used for scoria-rich samples. Subsequently, lithology was described using an optical microscope and fresh glass fragments were picked from selected samples for major-element characterization. As a criterion for the identification of cryptotephra, we selected those deposits where the juvenile fraction (mainly glass fragments) exceeded 50% of the bulk sediment.

Visible tephras were found in cores C14 (89–74 cm bsf) and UM42 (7.4–6.7 cm bsf). The selected sample in core C14 (C14/89) includes the 89–87 cm bsf interval characterized by prevailing volcanic materials (Table 1). Sample UM42/7 was picked from the 6.7–7.1 cm bsf interval where scoria fragments represent 90% of the deposit (Table 1; Supporting Information Fig. S1).

In core CP10, the analyzed cryptotephra was recognized initially through elemental composition of the bulk sediments (Wu *et al.*, 2016, 2017). It was between 7 and 6.5 cm bsf (sample CP10/7) (Fig. S1).

In cores AP1 and C1, cryptotephras were identified by inspection of washed sediments (>63 μm fraction) used for foraminifera analysis. The deposit investigated in core AP1 occurs between 13 and 12 cm bsf (sample AP1/13), whereas in core C1, two cryptotephras are dispersed between 56 and 52 cm bsf (sample C1/56) and within the 90–80 cm bsf interval. The latter was subsampled at 1–2-cm steps to observe possible changes in lithology and the juvenile fraction content. Four subsamples (C1/82, C1/85, C1/87 and C1/90) were selected for chemical characterization.

Major element analysis

Juvenile fragments (pumice, scoria and glass shards) of samples selected from each deposit were mounted on epoxy resin and suitably polished for microprobe analyses performed on a JEOL JSM 5310 scanning electron microscope (15 kV, ZAF Correction Routine) equipped with an energy-dispersive spectrometer at DiSTAR (University of Naples "Federico II"). Operating conditions were 15-kV primary beam voltage, 50–100-mA filament current, 50-s acquisition time and variable spot size. Correction for matrix effects was performed using INCA version 4.08 software that used the XPP correction routine, based on a Phi-Ro-Zeta approach. Primary calibration was performed using international mineral and glass standards. Details on the standards used are given in Morabito *et al.* (2014). Precision and accuracy were assessed using the rhyolitic Lipari obsidian ID3506 and basaltic Laki 1783 AD tephra (Kuehn *et al.*, 2011) as secondary standards and the

Copyright © 2019 John Wiley & Sons, Ltd.

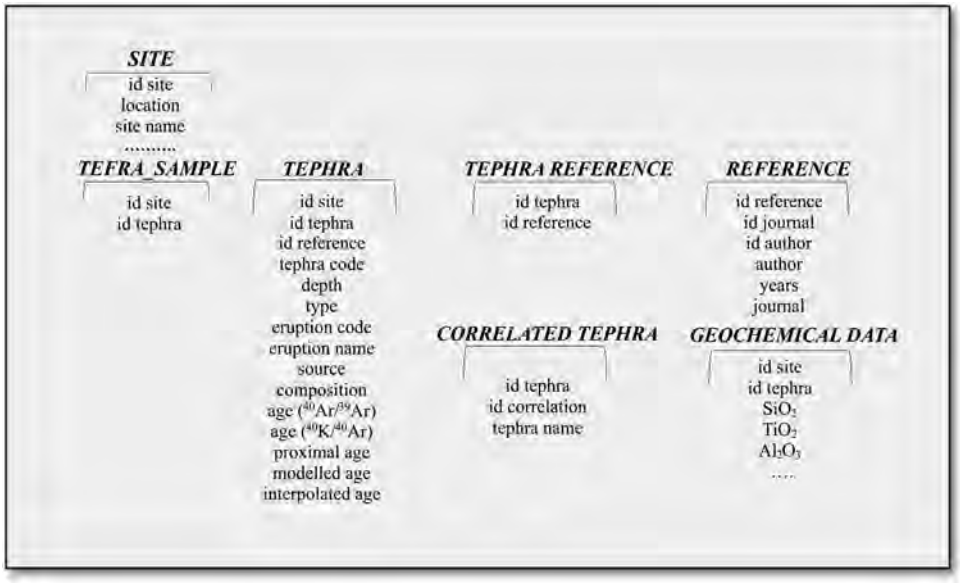

Figure 2. Entity recording data on tephra and cryptotephra in the WDB-Paleo database (Alberico *et al.*, 2017).

respective analytical values are reported in Supporting Information Table S1 along with analyses of individual glass fragments extracted from the studied deposits. Total oxide sums $\geq 93\%$ were deemed acceptable given that magmatic dissolved volatile components may reach >5% in evolved trachytes and rhyolites (e.g. Pearce *et al.*, 1999). Correlation of the analyzed tephra with proximal deposits or equivalents from different sites was based on a comparison of the new data with published scanning electron microscopy/energy-dispersive spectrometry (SEM-EDS) and wavelength-dispersice spectroscopy (WDS) data where available. The criteria used to infer the primary origin of the studied deposits are described in Insinga *et al.* (2014).

^{14}C AMS dating

Radiocarbon dating was performed by accelerator mass spectrometry (AMS) on planktonic foraminifera collected from five samples in stratigraphic association with the analyzed tephra. Measurements were performed at the Poznań Radiocarbon Laboratory, at the J. G. van de Graaff laboratory (Utrecht University) and at INFN-Labec of Florence following procedures described in Goslar *et al.* (2004), Van Der Borg *et al.* (1997) and Lubritto *et al.* (2018). All ^{14}C dates were converted into calendar ages using the Marine13 calibration curve (Reimer *et al.*, 2013) implemented in the program OxCal 4.3 (Bronk Ramsey, 2009) with no regional reservoir correction (i.e. $\Delta R = 0$), which is valid for the modern Mediterranean (Siani *et al.*, 2000).

The WDB-Paleo database

The WDB-Paleo database includes data on about 6000 cores recovered from the Mediterranean Sea (Alberico *et al.*, 2017). It hosts metadata concerning paleoclimatic proxies, stratigraphic and chronological data (planktonic and benthic foraminifera, pollen, calcareous nanoplankton, magnetic susceptibility, oxygen stable isotope, AMS ^{14}C dating and tephra layers) published in ca. 200 scientific publications with associated reference information (authors, journal, book, year, title). Quantitative proxy data from all cores acquired in the frame of a number of Italian research projects were also integrated along with metadata on tephras from continental archives of central–southern Italy used in this work. A new entity hosting geochemical data has been implemented with data obtained here as shown in the logical model reported in Fig. 2.

Results

Composition and sources of tephra

Lithological features of tephras (C14/89, UM42/7) and cryptotephras (C1/56, C1/80–90, AP1/13, CP10/7) are reported in Table 1. According to the total alkali–silica (TAS; Le Maitre, 2005) diagram and serial affinity (sodic to ultrapotassic), the analyzed samples are classified as basaltic trachyandesite, trachyphonolite and rhyolite, and from tephriphonolite to phonolite (Fig. 3a–c; Table 2). Tephras with Na-alkaline affinity occur in all cores except C14 (Fig. 3c). Two geochemical populations characterize tephra C14/89 (phonolite + trachyphonolite), and cryptotephras C1/85 (tephriphonolite-latite + mugearite), CP10/7 (rhyolite + mugearite) and AP1/13 (trachyphonolite + benmoreite) (Fig. 3). The overall chemical features of the analysed samples match well those of the Italian volcanic products and, in detail, with Mt Etna, Aeolian Arc *s.l.*, Somma-Vesuvius, Ischia Island and Campi Flegrei deposits (Fig. 3a,b; Table 1). These correlations are consistent with the location of the core sites, downwind and in the proximity of source vents.

Mt Etna related tephra

Deposits with Na-alkaline affinity (Fig. 3c) can be classified as mugearites, benmoreites and trachytes in the TAS diagram (Fig. 3a,b). These compositions are typical of the intermediate-evolved products erupted by Mt Etna volcano during the late Pleistocene–Holocene (Peccerillo, 2005) (Fig. 3a,b; Table 2). The analyzed tephras generally consist of fine ash, which displays a crystalline groundmass of juvenile materials with rare interstitial glass. Microlites are represented by clinopyroxene, plagioclase and opaques (Fig. 4a,b).

In core C1, the Etnean cryptotephra is dispersed in a relatively thick interval (ca. 10 cm) and it is characterized by a variable ratio between the content of juvenile fragments over the lithic and bioclastic fraction (Supporting Information Fig. S1). No evidence of reworking has been observed. The content of the juvenile fraction in the selected samples ranges from 70

Copyright © 2019 John Wiley & Sons, Ltd.

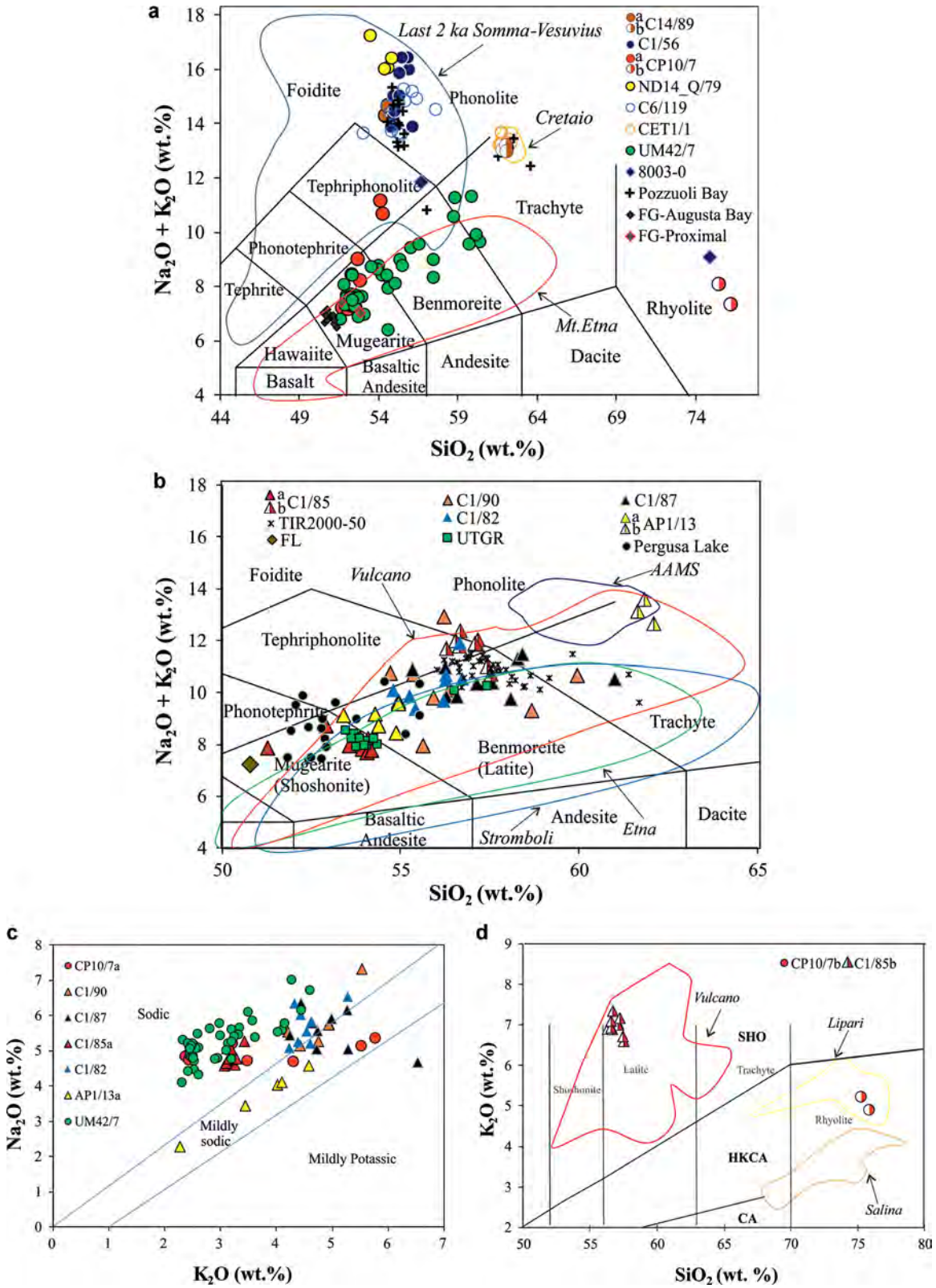

Figure 3. TAS classification diagrams (a,b) with composition of the studied tephras and cryptotephras. Compositional fields are labeled according to the Na- and K-series. The average compositional fields of proximal deposits and single glass data of some proximal and distal tephras are reported for comparison. Data for Somma-Vesuvius products are from Santacroce *et al.* (2008), Etna, Stromboli and Vulcano from Peccerillo (2005) and references therein, Cretaio from De Alteriis *et al.* (2010), FG proximal and Augusta Bay from De Martini *et al.* (2010) and Smedile *et al.* (2011), AAMS group from Smith *et al.* (2011), Upper Tufi di Grotte Rosse (UTGR) and TIR2000-50 from Albert *et al.* (2012), 8003-0 from Paterne *et al.* (1988), C6/199 from Di Donato *et al.* (2019), Pozzuoli Bay glasses from Sacchi *et al.* (2014), FG and FL from Coltelli *et al.* (2000, 2005). (c) K_2O/Na_2O diagram to show the Na-alkaline affinity of studied cryptotephra and (d) SiO_2/K_2O diagram to show the shoshonitic and HKCA features of cryptotephra CP10/7 and C1/85. Data for Salina and Lipari rhyolites are from Albert *et al.* (2017). [Color figure can be viewed at wileyonlinelibrary.com]

to 90% (C1/87 and C1/85) with respect to the biotic component in all the sieved fractions. Grayish pumice fragments occur with the ubiquitous dark scoria in sample C1/85. Glasses extracted from samples C1/90, C1/87 and C1/82 have a benmoreitic composition with some points also falling in the trachytic and tephriphonolitic field. In contrast, an almost homogeneous mugearitic glass (a), along with minor tephriphonolitic glass (b) characterize sample C1/85 (Fig. 4b).

Copyright © 2019 John Wiley & Sons, Ltd.

Table 2. Single glass chemistry for the studied tephra.

Core	CP10BC									AP1.1					C14								
Sample	CP10/7a							CP10/7b		AP1/13a					AP1/13b				C14/89a		C14/89b		
cm bsf	6.5–7									12–13					88–89								
SiO_2	53.91	54.04	52.50	52.20	52.71	51.57	51.92	75.29	75.91	54.90	54.81	54.09	54.25	53.31	61.76	61.29	61.48	54.95	54.50	54.65	62.12	62.14	61.93
TiO_2	1.78	2.06	1.76	1.65	1.68	1.76	1.98	0.00	0.00	2.42	1.75	1.88	1.84	2.15	0.65	0.49	0.35	0.40	0.59	0.55	0.68	0.71	0.66
Al_2O_3	16.08	15.81	16.02	16.67	18.25	17.00	17.26	13.67	13.14	16.16	19.34	16.68	16.72	15.37	18.52	18.30	18.57	20.64	20.42	20.62	18.49	18.53	18.38
FeO	8.79	8.24	8.84	8.71	8.30	9.50	9.04	1.41	1.57	9.04	6.37	8.00	8.74	10.13	3.12	3.70	2.85	3.87	4.19	3.95	3.13	2.87	3.24
MnO	0.27	0.39	0.22	0.33	0.04	0.27	0.12	0.00	0.00	2.12	1.71	2.90	2.70	0.02	0.64	0.57	0.34	0.10	0.37	0.25	0.17	0.09	0.00
MgO	2.42	2.56	3.31	2.96	2.58	3.49	3.59	0.00	0.21	0.00	0.21	0.28	0.00	3.36	0.41	0.17	0.32	0.28	0.16	0.24	0.37	0.40	0.51
CaO	3.52	4.07	6.48	6.84	7.01	7.75	7.29	0.76	0.92	4.69	6.18	5.53	5.65	4.93	1.64	1.64	2.03	3.90	4.36	4.23	1.45	1.48	1.52
Na_2O	5.34	5.12	4.67	5.18	4.70	4.81	4.71	2.87	2.41	6.10	6.15	5.08	4.59	4.50	4.61	4.19	5.34	4.68	4.71	4.88	5.90	6.05	6.09
K_2O	5.78	5.53	4.31	3.23	3.49	2.39	2.44	5.21	4.89	3.44	2.27	4.01	4.09	4.57	7.95	8.85	8.17	9.75	9.57	9.73	7.07	7.14	6.90
P_2O_5	1.27	1.21	1.08	1.60	0.70	0.87	0.97	0.19	0.00	1.02	1.11	1.18	1.15	1.46	0.11	0.18	0.00	0.00	0.13	0.16	0.06	0.20	0.10
Cl	0.42	0.48	0.41	0.31	0.28	0.30	0.34	0.30	0.47	0.11	0.12	0.36	0.28	0.21	0.60	0.61	0.55	0.87	0.82	0.72	0.51	0.40	0.44
Original total	97.59	99.83	97.69	98.23	96.40	97.38	96.17	95.88	95.31	97.38	100.87	97.28	97.49	100.22	96.11	94.79	98.07	98.49	97.43	98.12	97.47	96.78	98.77

Core	UM42BC																						
Sample	UM42/7																						
cm bsf	6.7–7.1																						
SiO_2	59.58	52.87	55.86	55.11	51.72	51.87	52.74	54.47	52.16	53.75	58.59	57.10	51.61	51.97	51.71	57.07	52.17	51.85	54.95	52.10	52.09	51.53	53.81
TiO_2	1.26	1.17	1.40	1.81	1.77	1.65	1.93	2.02	1.94	2.44	1.40	1.49	1.81	1.89	1.50	1.56	1.84	1.74	1.61	1.63	1.69	1.86	1.64
Al_2O_3	17.50	17.04	17.98	17.20	16.42	17.40	17.16	17.62	17.01	16.18	18.18	18.17	17.58	17.18	17.22	18.43	17.44	16.60	17.78	17.34	17.26	17.35	17.18
FeO	5.25	9.24	6.40	7.35	9.63	8.89	8.52	8.19	8.66	8.10	5.22	5.95	8.49	8.46	8.84	6.35	8.52	9.77	7.05	8.71	8.83	9.05	8.24
MnO	0.10	0.15	0.41	0.13	0.00	0.35	0.00	0.03	0.41	0.10	0.21	0.37	0.27	0.04	0.25	0.23	0.08	0.11	0.17	0.13	0.25	0.23	0.27
MgO	1.38	3.56	2.41	2.74	3.87	3.53	3.49	2.98	3.37	3.10	1.56	2.37	3.46	3.32	3.45	1.95	3.55	3.47	2.63	3.43	3.45	3.76	2.94
CaO	2.64	7.43	4.92	5.56	7.51	7.68	7.21	5.80	7.23	5.81	2.72	4.96	7.11	7.57	7.58	4.02	7.39	6.80	5.32	7.42	7.33	7.27	5.94
Na_2O	6.70	4.45	5.84	5.64	5.13	5.12	5.29	4.75	5.08	5.45	6.98	5.17	4.79	5.12	4.85	5.34	4.82	4.76	5.54	4.68	5.13	4.80	5.40
K_2O	4.58	2.52	3.56	3.32	2.52	2.47	2.32	3.18	2.59	3.31	4.25	3.11	2.42	2.44	2.42	3.58	2.47	2.93	3.17	2.49	2.42	2.50	2.97
P_2O_5	0.50	1.14	0.87	0.67	0.95	0.77	0.93	0.64	1.21	1.34	0.47	0.64	1.24	1.02	1.02	0.71	1.14	1.18	0.80	1.09	0.95	0.98	0.77
Cl	0.52	0.43	0.34	0.48	0.48	0.25	0.40	0.31	0.34	0.41	0.40	0.36	0.31	0.30	0.30	0.37	0.33	0.43	0.38	0.36	0.31	0.39	0.27
Original total	98.59	95.71	97.35	98.48	96.94	98.46	97.94	97.80	99.18	98.13	94.98	96.82	97.05	98.37	98.16	98.47	97.94	98.67	97.62	97.41	97.1	97.95	98.22

Core	UM42BC																						
Sample	UM42/7																						
cm bsf	6.7–7.1																						
SiO_2	52.21	52.27	52.13	53.55	52.02	51.93	54.02	51.90	52.36	59.66	52.08	59.63	54.70	59.22	58.32	53.98	55.85	51.13	51.34	53.13	51.89		
TiO_2	1.94	1.98	1.89	1.69	1.72	1.99	1.74	2.17	1.84	1.10	1.96	1.05	1.88	1.15	1.40	1.56	1.34	1.78	1.71	1.61	1.96		
Al_2O_3	16.49	16.73	16.96	17.00	17.00	17.25	18.15	17.18	17.11	18.79	17.06	18.66	17.51	18.88	18.04	17.38	18.02	17.41	17.26	17.23	16.49		
FeO	9.05	9.16	8.93	8.35	9.10	8.13	8.89	8.65	8.25	4.97	8.69	4.99	7.33	5.39	5.92	8.01	6.53	9.32	9.08	8.12	9.05		
MnO	0.17	0.17	0.13	0.09	0.05	0.24	0.17	0.15	0.25	0.14	0.18	0.21	0.25	0.15	0.16	0.17	0.23	0.28	0.00	0.21	0.19		

(*Continued*)

Copyright © 2019 John Wiley & Sons, Ltd.

Table 2. (*Continued*)

Core	UM42BC																				
Sample	UM42/7																				
cm bsf	6.7–7.1																				
MgO	3.72	3.63	3.59	3.00	3.66	3.46	1.97	3.67	3.55	1.31	3.64	1.39	2.99	1.38	1.47	2.81	2.23	3.81	3.47	2.99	3.17
CaO	7.24	7.37	7.14	6.03	7.40	7.86	6.77	7.22	7.44	3.08	7.44	2.98	5.71	3.24	2.92	5.80	4.53	7.65	7.16	6.19	7.08
Na_2O	4.74	4.28	5.17	5.38	4.75	5.18	4.05	5.03	5.09	5.51	5.02	5.74	4.98	5.49	6.10	5.20	6.03	4.38	5.42	5.74	5.58
K_2O	2.89	2.58	2.47	3.21	2.49	2.40	2.28	2.54	2.46	4.06	2.44	4.12	3.09	4.00	4.41	3.17	3.45	2.40	2.57	2.95	2.78
P_2O_5	0.89	0.99	0.80	0.98	0.93	0.84	0.87	0.95	0.93	0.22	0.94	0.36	0.93	0.27	0.54	0.86	0.56	0.95	1.05	1.10	0.93
Cl	0.31	0.35	0.35	0.33	0.25	0.28	0.25	0.26	0.25	0.51	0.32	0.41	0.35	0.45	0.41	0.30	0.34	0.32	0.35	0.27	0.36
Original total	96.67	97.82	98.86	98	97.75	98.35	96.03	97.28	95.99	97.65	98.31	97.20	95.45	96.83	98.34	99.69	99.99	98.71	98.45	94.6	95.64

Core	C1																		
Sample	C1/90									C1/87									
cm bsf	88–90									86–87									
SiO_2	56.04	54.51	54.57	55.99	55.67	55.37	55.50	59.89	58.59	57.27	56.92	57.82	57.97	55.96	55.88	56.15	60.55	54.99	58.11
TiO_2	1.97	1.83	1.86	1.59	1.61	1.94	1.55	2.02	1.61	1.60	1.64	1.88	1.77	1.26	1.67	1.78	1.05	1.84	1.34
Al_2O_3	17.37	16.64	16.18	16.64	17.60	15.70	15.70	16.83	16.02	16.85	16.48	18.29	18.30	17.89	17.80	16.70	18.83	17.34	17.56
FeO	5.53	8.13	9.59	7.78	7.77	8.28	8.79	4.53	5.91	7.76	6.60	6.21	6.82	7.62	7.88	7.92	4.64	7.45	5.92
MnO	0.20	0.23	0.13	0.37	0.34	0.22	0.48	0.00	0.28	0.60	0.42	0.34	0.18	0.25	0.18	0.28	0.14	0.27	0.08
MgO	1.19	2.29	2.33	2.12	2.15	2.32	2.04	1.03	1.57	1.38	2.08	0.89	0.77	1.28	1.58	1.40	0.97	2.44	1.19
CaO	2.97	4.28	3.91	3.60	3.40	3.89	6.60	3.84	5.44	2.66	4.44	3.64	1.96	3.03	3.34	3.77	1.96	3.09	2.71
Na_2O	7.31	5.75	5.15	5.26	5.54	5.73	5.76	6.08	6.44	5.03	5.55	5.44	4.67	5.90	5.05	5.04	5.77	6.34	6.15
K_2O	5.54	4.95	4.43	4.76	4.20	4.94	2.13	4.56	2.82	5.29	4.75	4.24	6.53	4.98	4.73	4.73	4.65	4.44	5.26
P_2O_5	1.51	1.00	1.14	1.18	1.28	1.60	1.19	1.11	1.14	1.00	0.71	0.77	0.46	1.29	1.17	1.45	0.70	1.18	1.13
Cl	0.37	0.41	0.71	0.71	0.44	0.00	0.25	0.11	0.18	0.54	0.41	0.48	0.56	0.55	0.74	0.77	0.75	0.63	0.55
Original total	95.85	100.06	99.50	97.29	101.33	99.42	99.30	98.08	99.38	99.78	101.99	102.54	101.56	95.97	94.94	95.71	94.91	92.57	91.74

Core	C1																				
Sample	C1/85a												C1/85b								
cm bsf	84–85																				
SiO_2	51.21	52.83	53.90	53.94	53.80	53.90	54.02	53.80	53.40	53.73	57.36	57.26	57.00	56.43	56.37	56.88	56.55	57.02	56.51	56.15	
TiO_2	1.75	2.10	1.73	1.68	1.94	1.99	1.85	2.01	2.00	1.69	0.72	0.52	0.71	0.87	0.66	0.77	0.79	0.46	0.73	0.74	
Al_2O_3	16.91	16.65	17.13	17.03	17.26	17.47	17.31	16.96	17.20	17.28	18.89	18.57	18.33	18.25	18.53	18.38	18.52	18.04	18.15	18.02	
FeO	10.36	8.38	8.62	8.99	8.78	8.49	8.90	8.89	9.01	8.82	6.10	6.02	5.91	6.19	6.17	6.04	5.82	6.12	6.29	6.22	
MnO	0.28	0.09	0.26	0.12	0.16	0.28	0.05	0.15	0.27	0.26	0.00	0.03	0.22	0.34	0.31	0.00	0.05	0.21	0.11	0.19	
MgO	4.22	3.09	3.07	3.33	3.00	3.11	3.02	2.90	2.96	3.13	1.69	1.75	1.63	1.72	1.60	1.52	1.61	1.71	1.81	2.01	
CaO	6.39	7.01	6.01	5.46	6.09	5.86	5.87	5.92	6.01	5.67	3.81	4.07	3.63	3.38	3.51	3.72	3.77	3.65	3.91	4.22	
Na_2O	4.58	5.25	4.73	5.06	4.69	4.55	4.64	4.76	4.76	5.03	4.07	4.29	4.84	4.93	5.02	4.81	5.01	4.85	4.88	4.76	
K_2O	3.26	3.42	3.19	3.11	3.11	3.06	3.09	3.29	3.14	3.19	6.57	6.68	6.96	7.08	6.91	7.02	7.32	7.12	6.87	6.88	
P_2O_5	0.90	0.99	1.04	0.97	0.92	0.98	0.94	1.04	0.93	0.94	0.46	0.49	0.52	0.51	0.66	0.61	0.33	0.51	0.47	0.53	
Cl	0.15	0.20	0.31	0.30	0.26	0.30	0.30	0.27	0.30	0.26	0.33	0.31	0.24	0.29	0.26	0.25	0.24	0.30	0.25	0.28	
Original total	95.99	95.86	95.33	96.31	99.73	96.60	96.63	98.57	95.46	96.13	98	95.84	94.40	96.32	95.48	95.34	95.23	97.16	97.07	95.75	

(*Continued*)

Copyright © 2019 John Wiley & Sons, Ltd.

Table 2. *(Continued)*

Core	C1																	
Sample cm bsf	C1/82 80–82						C1/56 52–56											
SiO_2	56.23	54.73	55.02	55.92	55.02	56.46	55.95	56.37	54.61	54.49	54.80	54.55	54.54	55.88	55.51	55.52	54.96	54.70	54.90	55.15
TiO_2	1.87	1.94	1.99	1.67	2.03	2.02	1.77	1.81	0.33	0.49	0.49	0.47	0.39	0.09	0.41	0.25	0.50	0.56	0.30	0.14
Al_2O_3	16.89	16.16	15.97	17.11	16.74	17.58	18.45	17.22	19.80	20.96	21.30	21.36	20.38	21.18	22.32	22.05	22.58	20.51	21.71	22.35
FeO	7.36	8.89	10.00	8.66	8.99	7.61	8.29	6.53	4.31	3.56	2.93	3.27	3.80	3.40	2.45	2.02	2.57	4.16	2.72	2.24
MnO	0.26	0.27	0.29	0.23	0.39	0.03	0.10	0.34	0.00	0.28	0.32	0.06	0.17	0.00	0.00	0.07	0.33	0.17	0.00	0.06
MgO	1.92	2.26	2.06	1.59	2.12	1.71	1.18	1.46	0.71	0.46	0.51	0.52	0.54	0.63	0.12	0.07	0.12	0.67	0.29	0.14
CaO	3.48	4.04	3.31	3.63	3.62	2.64	2.25	2.52	5.53	5.17	3.71	4.07	4.94	4.38	2.59	3.04	3.15	4.22	3.54	2.94
Na_2O	6.33	5.55	5.19	5.24	5.07	6.03	5.81	6.54	5.53	6.12	5.53	5.77	5.04	5.60	6.73	7.32	6.74	5.01	7.08	6.75
K_2O	4.32	4.54	4.61	4.39	4.23	4.44	4.63	5.27	8.36	7.69	9.51	9.14	9.11	8.23	9.13	8.99	8.17	9.36	8.67	9.58
P_2O_5	1.23	1.52	1.11	1.03	1.08	1.01	0.98	1.41	0.00	0.12	0.30	0.00	0.31	0.06	0.00	0.00	0.17	0.00	0.00	0.00
Cl	0.10	0.10	0.46	0.52	0.71	0.46	0.59	0.53	0.82	0.66	0.61	0.79	0.77	0.55	0.74	0.66	0.70	0.63	0.79	0.65
Original total	100.46	95.63	97.62	98.79	98.75	100.37	99.40	97.5	95.96	99.05	100.88	96.70	95.38	95.33	97.75	97.39	99.35	99.31	100.58	97.32

All the analyses recalculated free water to 100. The original totals have been also reported.

Tephra AP1/13 has a benmoreitic-mugearitic composition (a) and is associated with a minor trachyphonolitic glass (b).

Tephra UM42/7 is the only visible layer among the Etnean products. The deposit is well preserved and includes a fresh juvenile fraction exceeding 85% of the whole lithic and biotic content. The juvenile materials are represented by aphyric and microlite-bearing glass shards (Fig. 4c) and a minor component of porphyritic scoriae (Table 1). A larger compositional variability characterizes this deposit, which has a mugearitic, benmoreitic and trachytic composition. Trachytic points with SiO_2 concentration up to ca. 60 wt% are observed in aphyric glasses.

Tephra CP10/7 is characterized by a mugearitic population (a) with two glass fragments falling in the tephriphonolite field.

Aeolian Arc related tephra

Glass shards of cryptotephra CP10/7 appear light in color and characterized by a platy morphology under optical observation. They have a rhyolitic composition (b) with a high-K calc-alkaline (HKCA) affinity typical of Lipari deposits erupted during the Late Pleistocene–Holocene (Fig. 3d; Table 2). Cryptotephra C1/85b is a tephriphonolite with shoshonitic (SHO) affinity (Fig. 3d; Table 2). Glasses are dark yellow and display a blocky morphology. Major element composition is fairly homogeneous: SiO_2 values range from 56.3 to 57.6 wt%, FeO_{tot} from 5.8 to 6.3 wt%, CaO from 3.4 to 4.23 wt% and TiO_2 from 0.46 to 0.87 wt%. Volcanic products with such chemical composition have been erupted both by Stromboli and by Vulcano during the Holocene (Fig. 3b).

Somma-Vesuvius, Ischia and Campi Flegrei related tephra

Tephra C14/89 is 15 cm thick and formed by a medium-grained ash lying on a sharp erosive basal contact. Towards the top of the deposit, laminated structures containing biotite and lithics can be observed and the glass fraction decreases significantly over the lithic, crystal and bioclastic portion. Chemically, a phonolitic composition (a) coexists with a trachyphonolitic one (b) (Fig. 3a); both are very homogeneous in terms of major oxide concentration (Table 2). The phonolitic shards are characterized by average SiO_2 values of ca. 54.7 wt %, Al_2O_3 of ca. 20.5 wt%, Na_2O of ca. 4.7 wt%, K_2O of 9.7 wt % and FeO_{tot} of ca. 4.01 wt%. The trachyphonolitic glass shards display average SiO_2 values of ca. 62 wt%, CaO of ca. 1.5 wt% and $Na_2O/K_2O = 0.85$. According to these chemical features, the phonolitic and trachyphonolitic populations of tephra C14/89 can be related to the highly and mildly silica-undersaturated potassic series of rocks (Fig. 3a,b) erupted by Somma-Vesuvius and Ischia volcanoes, respectively, during the Holocene (e.g. Conticelli *et al.*, 2010).

Cryptotephra C1/56 is a fine ash consisting of mostly light gray micropumice. Leucite-bearing scoria and lithic fragments, obsidian, blocky glass shards and loose crystals also occur (Table 1). The glass fragments have a phonolitic composition (Fig. 3a; Table 2) with SiO_2 values ranging from 54.8 to 56.2 wt%, Al_2O_3 from 20 to 22.74 wt%, Na_2O from 5 to 7.37 wt% and CaO from 2.6 to 5.6 wt%. Lithological features (e.g. occurrence of leucite) and composition suggest a correlation of C1/56 with Somma-Vesuvius deposits.

The minor trachyphonolitic component (b) occurring in cryptotephra AP1/13 is characterized by an average SiO_2 value of 61.5 wt%, Al_2O_3 of ca. 18.46 wt% and $K_2O/Na_2O = 1.77$. These analyzed points display mildly

Copyright © 2019 John Wiley & Sons, Ltd.

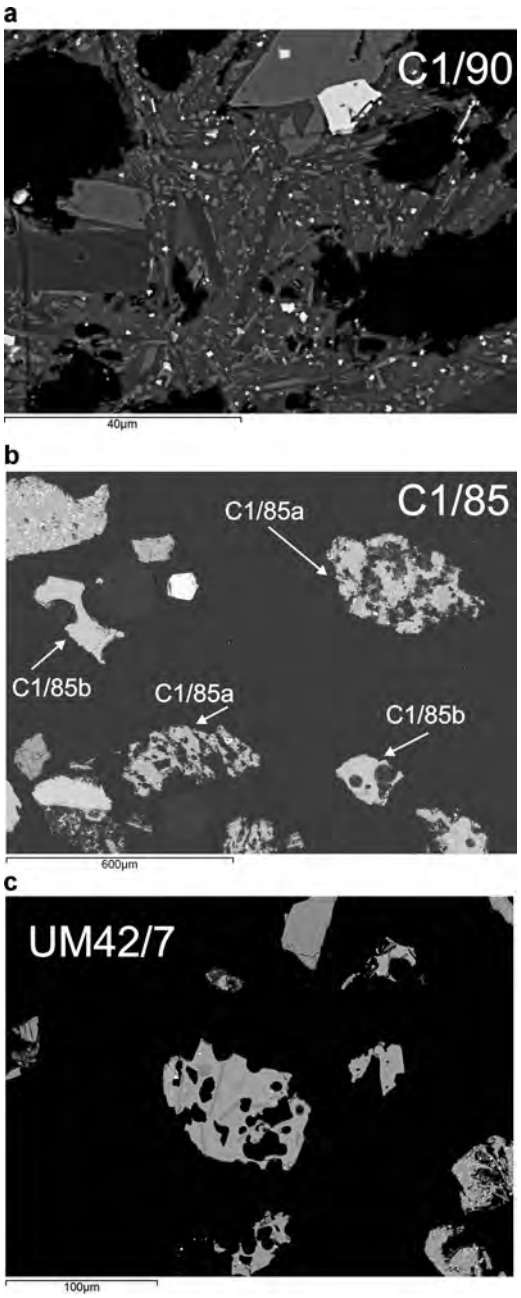

Figure 4. SEM images of samples C1/90 and C1/85 to show (a) the microlitic content of groundmass and the rare interstitial glass of Etnean tephra, (b) the two coexisting glass types with different morphologies in C1/85 and (c) the porphyritic scoriae occurring with microlite-bearing and aphyric glasses in tephra UM42/7.

silica-undersaturated potassic compositions typical of Campi Flegrei products.

Age of tephra

AMS ^{14}C dates from cores C1, AP1, UM42 and CP10 are reported in Table 3. They are consistent with the stratigraphic position of the picked samples. Cryptotephra occurring in core C1 from 80 to 90 cm bsf is chronologically constrained by an age of 3625 ± 96 cal a BP obtained from a 2-cm-thick sample immediately below the deposit. Tephra UM42/7 occurs ~1 cm below sample DD01317 located at (on average) 5.65 cm bsf and dated at 1797 ± 56 cal a BP. Because cosmogenic nuclide measurements indicate negligible loss of material from the core top (our unpublished data), the mean sedimentation rate (SR) for the stratigraphic interval can be estimated at ca. 3 cm ka^{-1}. Extrapolating this SR down in the section for the very first

Table 3. Summary of AMS ^{14}C dates on planktonic foraminifera extracted from core samples.

Core	Sample	Lab no.	Sample type	Sampling depth from top of core (cm)	Depth of tephra from top of core (cm)	Radiocarbon age (a BP) 2σ	Calibrated age (cal a BP)
C1	C1/90-92	FI4084	Mixed planktonic foraminifera	90–92	80–90	3702 ± 71	3625 ± 96
AP1	GG0123	Poz-82785	*G. ruber*	7–8	12–13	2590 ± 30	2260 ± 49
AP1	GG0130	Poz-82786	*G. ruber*	14–15		4570 ± 35	4777 ± 53
UM42	DD01317	UtC-8625	*G. ruber*	5.4–5.9	6.7–7.4	2202 ± 41	1797 ± 56
CP10BC	#25 + #26	Poz-55177*	*G. ruber* and *G. sacculifer*	6–6.5	6.5–7	2280 ± 30	1890 ± 44
CP10BC	#37 + #38	Poz-74801	*G. ruber* and *G. sacculifer*	9–9.5		3255 ± 35	3075 ± 60

* From Wu *et al.* (2016).

Copyright © 2019 John Wiley & Sons, Ltd.

few centimeters, we infer an age of ~2.2 cal ka for tephra UM42/7. The OxCal U_Sequence function (' ', 10) (Bronk Ramsey, 2008) was used to obtain a linear interpolated age for cryptotephras AP1/13 and CP10/7 constrained above and below by two radiocarbon ages (Table 3). This procedure yielded an age of 4237 ± 44 cal a BP for AP1/13 and of 2187 ± 37 cal a BP for UM42/7. The estimated SRs for the stratigraphic intervals containing the two cryptotephra are ca. 3 and 2.5 cm ka^{-1}, respectively.

Discussion

Proximal counterparts and marine equivalents

The tephrostratigraphic results and AMS ^{14}C ages are discussed for the studied deposits grouped according to their source vent. Most of the tephras and cryptotephras are correlated with age-dated volcanic events on land and/or with marine correlative layers in the central Mediterranean. Cross-correlations reveal the occurrence of two main marker tephras, whereas other deposits have been recognized for the first time in the marine setting (Fig. 5).

Somma-Vesuvius, Ischia and Campi Flegrei

The phonolitic composition of C14/89a and C1/56 indicates Somma-Vesuvius as the source volcano and Pompeii 79 AD (Sigurdsson *et al.*, 1985) as the source eruption (Figs 3 and 6). This event is widely recognized in areas adjacent to the C14 core site in the Pozzuoli Bay (Sacchi *et al.*, 2014) and to the C1 core site offshore Capo Vaticano (Cosentino *et al.*, 2017) (Fig. 1). The lithology of tephra C14/89 in core C14 is distinctive of Pompeii deposits in the Naples and Pozzuoli bays. Sedimentological features include a significant thickness, an erosive bottom surface and parallel laminations, which suggest possible syneruptive reworking (Sacchi *et al.*, 2005; Insinga *et al.*, 2008). The correlation of cryptotephra C1/56 with Pompeii products is supported by its stratigraphic position in the C1 record above tephra unit C1/90-82 (ca. 3.6 cal ka BP; Table 1). According to the FeO_{tot} versus CaO diagram (Fig. 6a), a continuous compositional variation trend from 79 AD gray to white pumice is observed in C1/56, whereas other distal equivalents display a single and/or two-fold clusters. This includes C14/89a glass shards which display the gray pumice composition, and cryptotephra ND14_Q/79 from the southern Adriatic that is characterized by the white pumice chemistry (Figs 1,6).

The Ischia glass population of tephra C14/89b matches well with Cretaio deposits (Orsi *et al.*, 1992) (Fig. 3a), widely dispersed offshore of the island (De Alteriis *et al.*, 2010). A number of radiocarbon datings from terrestrial and marine setting locate this event between 85 BC and 423 AD (Table S2). However, this large interval can be reasonably limited to the 1st century AD according to stratigraphic evidence from the marine settings, i.e. the amalgamation of Cretaio and Pompeii deposits observed in Pozzuoli Bay (Sacchi *et al.*, 2014) and in the southern Tyrrhenian (CET1 core site; Morabito *et al.*, 2014) (Figs 3 and 6).

The Campi Flegrei cryptotephra AP1/13b (4237 ± 44 cal a BP) can be correlated with the intense activity that occurred during the Late Holocene and produced mostly trachyphonolitic

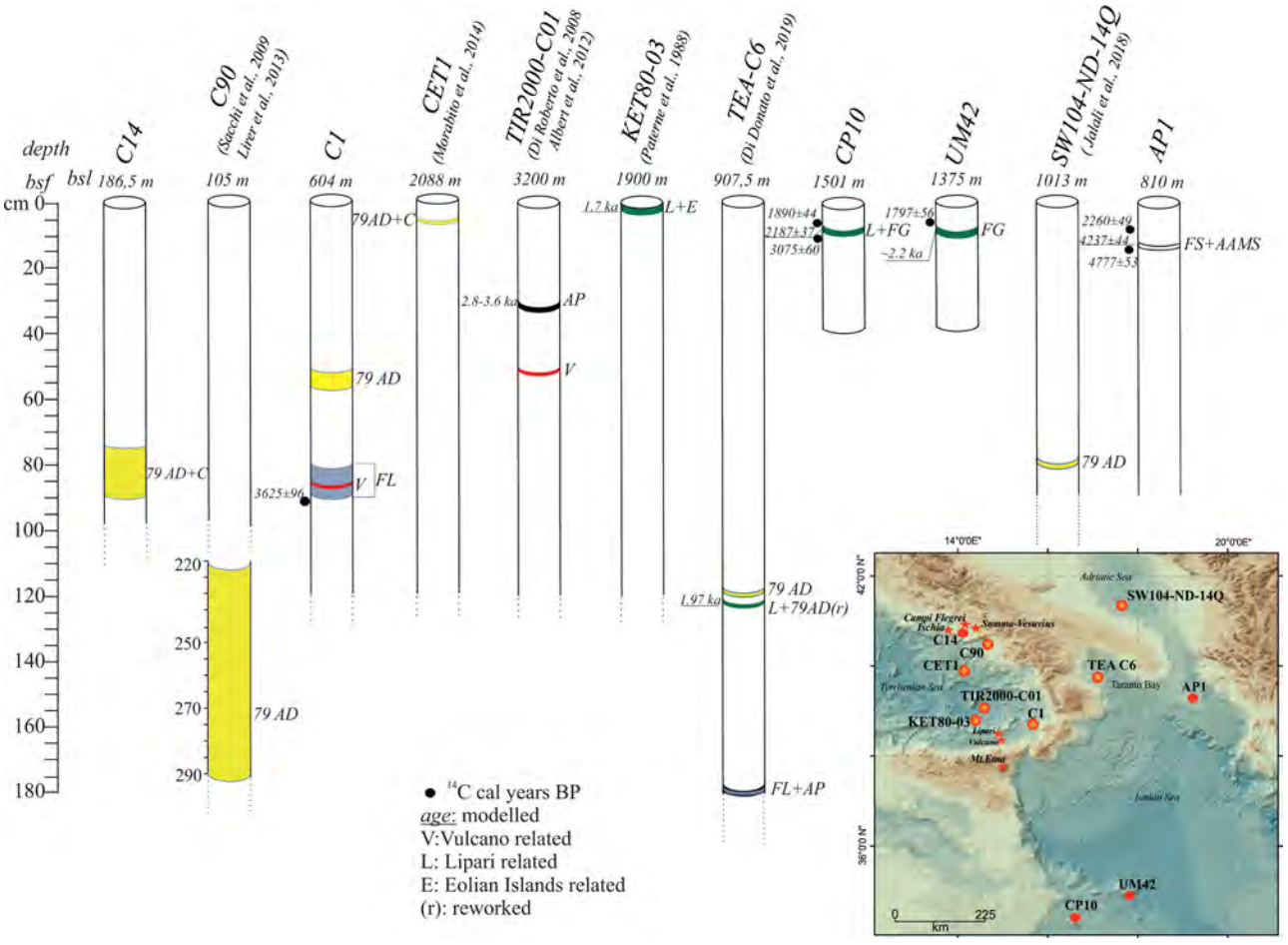

Figure 5. Tephrostratigraphy of the studied records for the 4.4 ka to 1st century AD time interval. Distal equivalents and source events from some cores in the southern Tyrrhenian, Gulf of Taranto and Adriatic Sea have been reported and discussed in the text. Reference cores may contain other tephra which have not been recalled here. [Color figure can be viewed at wileyonlinelibrary.com]

Copyright © 2019 John Wiley & Sons, Ltd.

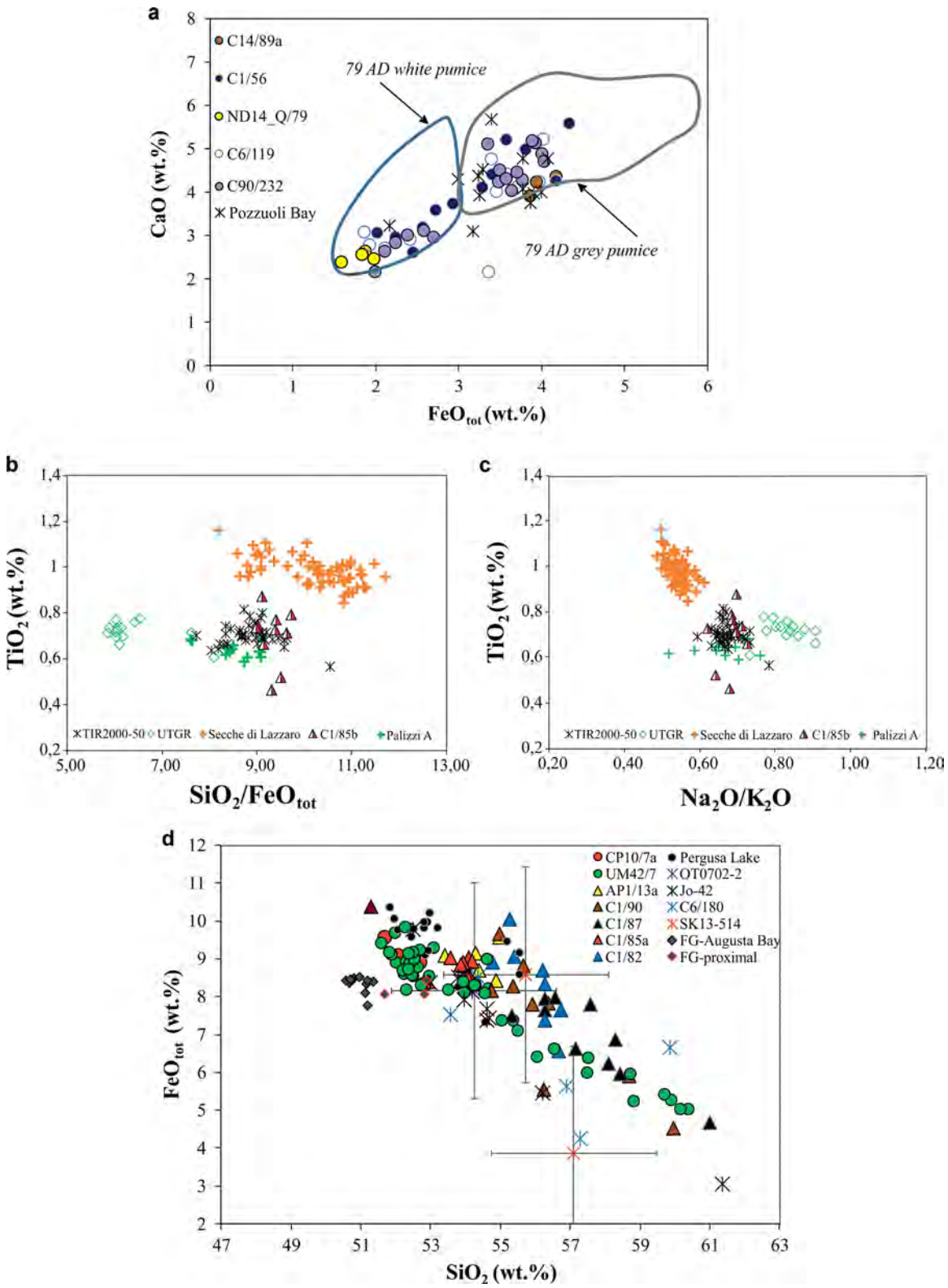

Figure 6. Binary diagrams with composition of tephras and cryptotephras compared with proximal counterparts and medial–distal equivalents. (a) FeO_{tot} vs CaO diagram with tephra C14/89a and the 79 AD white and gray pumice from the proximal site. Data from Santacroce *et al.* (2008), Sacchi *et al.* (2014) – Pozzuoli Bay tephra, Jalali *et al.* (2018) – ND14_Q/79, Di Donato *et al.* (2019) – C6/119, Lirer *et al.* (2013) – C90/232. (b) SiO_2/FeO_{tot} vs TiO_2 and (c) Na_2O/K_2O vs TiO_2 diagrams with composition of cryptotephra C1/85b, Stromboli (Secche di Lazzaro) and Vulcano (Palizzi A and UTGR) deposits and the marine TIR2000-50. Data from Albert *et al.* (2012, 2017). (d) SiO_2 vs FeO_{tot} diagram with Etnean cryptotephra analyzed in this work and compared with mid- and distal FG and FL equivalents. Single glass data are from Sadori *et al.* (2013) – Pergusa Lake, Vogel *et al.* (2010) – OT07702-2 (Lake Ohrid), Caron *et al.* (2010) – Jo-42 (Lake Ohrid), Sulpizio *et al.* (2010) – SK13-514-average (Lake Shkodra), De Martini *et al.* (2010) and Smedile *et al.* (2011) – FG proximal and Augusta Bay. [Color figure can be viewed at wileyonlinelibrary.com]

products. Their homogeneous composition in terms of major elements makes discrimination very difficult (Smith *et al.*, 2011). This is particularly true for the Agnano Mt Spina and Astroni eruptions (AAMS group) reported between ca. 4.4 and 4.6 cal ka BP and between ca. 4.1 and 4.3 cal ka BP at proximal sites, respectively (Smith *et al.*, 2011). In the marine setting, robust ages of 4166 ± 114 cal a BP for Astroni tephra and 4422 ± 58 cal a BP for Agnano Mt Spina tephra are provided by radiocarbon

Copyright © 2019 John Wiley & Sons, Ltd.

dating and age–depth modeling (Siani *et al.*, 2004; Lirer *et al.*, 2013) (Table S2). Distal products of the AAMS group may occur either as multiple layers or amalgamated within one or more horizons (Siani *et al.*, 2004; Crocitti *et al.*, 2018). Although a discrimination criterion based on major element chemistry has been proposed (Margaritelli *et al.*, 2016), the very low amount of glass shards found in the deposit hampers any robust statistical analysis and hence we prefer to maintain a generic attribution of AP1/13b to the AAMS group.

Lipari

Two HKCA rhyolitic glass shards occur in CP10/7b dated at 2187 ± 37 cal a BP. Distal cryptotephras with such a rhyolitic composition and a similar age have been found in cores KET80-03 (Paterne *et al.*, 1988) and TEA C6 (Di Donato *et al.*, 2019) in the southern Tyrrhenian Sea and in the Gulf of Taranto, respectively (Fig. 5). In detail, a main Lipari rhyolitic population occurs at the top of core KET and it coexists with Aeolian tephriphonolites (Fig. 3a) dated at ca. 1.7 ka based on sapropel chronology and isotope stratigraphy. In core TEA C6, cryptotephra C6/122 occurs immediately below the 79 AD tephra (C6/119) and it includes HKCA rhyolites with few reworked Pompei micropumice (Fig. 3a) dated at 1.97 cal ka BP according to an age–depth model age constrained by tephrochronology and AMS ^{14}C dates. The proximal–distal correlation of this widespread deposit is hampered by the chronostratigraphy because no volcanic event is reported on the island at ca. 2 ka (e.g. Forni *et al.*, 2013).

Vulcano

According to the TAS and binary diagrams (Figs 3,6), we suggest a correlation of the tephriphonolitic (SHO) C1/85b with activity at Vulcano Island. This is supported by the TiO_2 and Na_2O concentration of Vulcano deposits, which display slightly different composition with respect to Stromboli shoshonitic products (Albert *et al.*, 2017). Tephra TIR2000-50 in the Marsili Basin (Di Roberto *et al.*, 2008; Albert *et al.*, 2012) is likely to be the marine equivalent of C1/85b (Figs 5 and 6). It occurs in core TIR2000-C01 stratigraphically below the Avellino–Pompeii (**AP**) interplinian deposits erupted at Somma-Vesuvius with age generally reported between 2.8 and 3.6 ka (Di Roberto *et al.*, 2008). The proximal–distal correlation of TIR2000-50 was discussed by Albert *et al.* (2012, 2017) but remained unresolved. Although a perfect chemical match can be observed between C1/85b and TIR2000-50 with 'Palizzi A' products emplaced at Vulcano at ca. 2 ka (Voltaggio *et al.*, 1995) (Fig. 6b,c), this correlation contrasts with the age of 3625 ± 96 cal a BP obtained just below our cryptotephra. Considering older activity on the island, a possible correlation with the Tufi di Grotte dei Rossi formation, constrained at ca. 4–5 ka (Lucchi *et al.*, 2008 and references therein), could have been hypothesized but the less evolved composition of these Vulcano deposits with respect to C1/85b excludes this possibility (Fig. 6b,c). In conclusion, tephra C1/85b-TIR2000-50 represents an as yet unknown event.

Mt Etna

During the last 4 ka, intense volcanism at Etna has produced a large number of tephras (Coltelli et al., 2000). Among these are regional marker beds documented on land in the ca. 4.3–2.0 ka time span and known as tephras FS, FL, FG and FF (Coltelli *et al.*, 1998, 2000, 2005). Tephras FL and FG are reported at medial–distal sites in both marine and terrestrial settings, whereas no records have yet been documented for the other deposits outside the perivolcanic area. The attribution of distal deposits to tephras FL and FG relies mostly on their overall Etnean compositional affinity and age constraints. This is mostly due to the insufficiency of data available on these proximal deposits in terms of single glass shard chemistry. This paucity reflects the difficulties when comparing different datasets (generally bulk versus single glass analysis) to establish proximal–distal correlations and recognize the eruptive event (Insinga *et al.*, 2014). Moreover, the microlite-rich groundmass and the rare interstitial glass, which are typical features of these Etnean deposits (Coltelli *et al.*, 2000), make their chemical characterization a difficult task even at proximal sites. Our results are focused on more comprehensive single glass chemistry and dispersal in offshore areas and, in this context, they provide a new contribution towards a better understanding of these Late–Holocene Etnean deposits.

The benmoreitic cryptotephra AP1/13a represents the oldest Etnean deposit of this study. According to the age of 4237 ± 44 cal a BP and an SR value of 3 cm ka^{-1} for the analyzed stratigraphic interval, the studied deposit can probably be correlated with the FS subplinian eruption dated at 4360 ± 92 cal a BP on land (Coltelli *et al.*, 2000, 2005).

The compositional field shown by subsamples of cryptotephra dispersed in the interval 90–80 cm bsf in core C1 (Figs 3,6) and the age result of 3625 ± 96 cal a BP immediately below suggest a correlation of the deposit with the FL event, a complex phreatomagmatic eruption dated on land at 3361 ± 76 cal a BP (Coltelli *et al.*, 2000). At distal sites, the FL fall products display large chemical variability and may coexist with the AP deposits (Pepe *et al.*, 2018; Di Donato *et al.*, 2019) (Figs 5,6). At Lago di Pergusa, south-east of Mt Etna (Fig. 1), where FL distal tephra was recognized for the first time and dated at ca. 3.3 cal ka BP (Sadori and Narcisi, 2001), single glass shards, instead, display a mugearitic composition close to that of C1/85a (Figs 3,6). Considering these observations along with the significant thickness in core C1, we infer that our cryptotephra may include the whole FL event. It was a long-lasting eruption, probably older than ca. 3.3 cal ka BP, characterized by significant chemical variability and different dispersal of products. However, further comparisons with proximal deposits and datings are required to verify this working hypothesis.

According to the age of ca. 2.2 cal ka BP, tephra UM42/7 may be regarded as the distal counterpart of tephra FG dated between 380 BC and 120 AD and ascribed to the historical 122 BC Plinian event (Coltelli *et al.*, 1998) (Table S2). Eruptive products were dispersed mainly towards the south-east and marine findings are reported in Augusta Bay (De Martini *et al.*, 2010; Smedile *et al.*, 2011) and Malta Plateau (Micallef *et al.*, 2016) (see Fig. 8). Proximal and medial–distal glass data indicate a homogeneous mugearitic composition of FG tephra (Fig. 3a), whereas at the UM42 site the deposit reveals a wider chemical variability, which characterizes also other Etnean deposits at distal sites (Fig. 6d). For now, we suggest UM42/7 as the reference distal tephra of FG deposits for future correlations and further geochemical studies.

Considering the comparable age and the mugearitic composition (Figs 3,6) along with the low SRs of cores CP10 and UM42 for the investigated time interval (2.5 and 3 cm ka^{-1}, respectively), a correlation of cryptotephra CP10/7 with UM42/7 and therefore with FG tephra is likely. This inference is also supported by the dispersal direction and volume of the 122 BC tephra, which is much higher than that of the almost coeval 44 BC tephra (Coltelli *et al.*, 2000).

Copyright © 2019 John Wiley & Sons, Ltd.

Tephra occurrences in the central Mediterranean Sea during the 4.2–2.0 ka time interval

Tephra correlation and dating results from this study have been included in the WdB-Paleo database in order to draw maps showing the occurrences of marker and minor tephra and newly discovered deposits in the central Mediterranean Sea (Figs 7,8). Moreover, other major tephra, erupted during the investigated time interval but not occurring in our cores, have also been considered and mapped to provide a general overview of their distribution (Fig. 7). These are namely the Somma-Vesuvius related Avellino (3945 ± 10 cal a BP; Sevink *et al.*, 2011) and AP1-6 (ca. 2.8–3.6 cal ka BP; Santacroce *et al.*, 2008 and references therein) tephras, which represent important correlation tools given their significant areal distribution over southern Italy and surrounding seas (Fig. 7). If there is a general consensus on the proximal–distal correlation of the Avellino tephra across the basin, large uncertainty remains when attempting discrimination among the six AP events. This is probably due to their often overlapping chemical composition and insufficient chronological constraints, particularly concerning the AP3-6 eruptive units, commonly reported as younger than ca. 2.8 cal ka BP according to a single radiocarbon age (Table S2). However, recent results from the marine setting point to an aging of the AP3-6 cluster as suggested by age–depth models (Sacchi *et al.*, 2009; Lirer *et al.*, 2013) (Table S2) and the finding of these deposits in association with FL tephra at distal sites (Pepe *et al.*, 2018; Di Donato *et al.*, 2019). According to these considerations, an age interval of ca. 3.6–3.4 cal ka BP for the AP eruptive sequence can be regarded as a working hypothesis to be further developed.

The maps obtained from the WdB-Paleo database provide a contribution to previous studies having implications for ash dispersal hazards related to both major and minor explosive

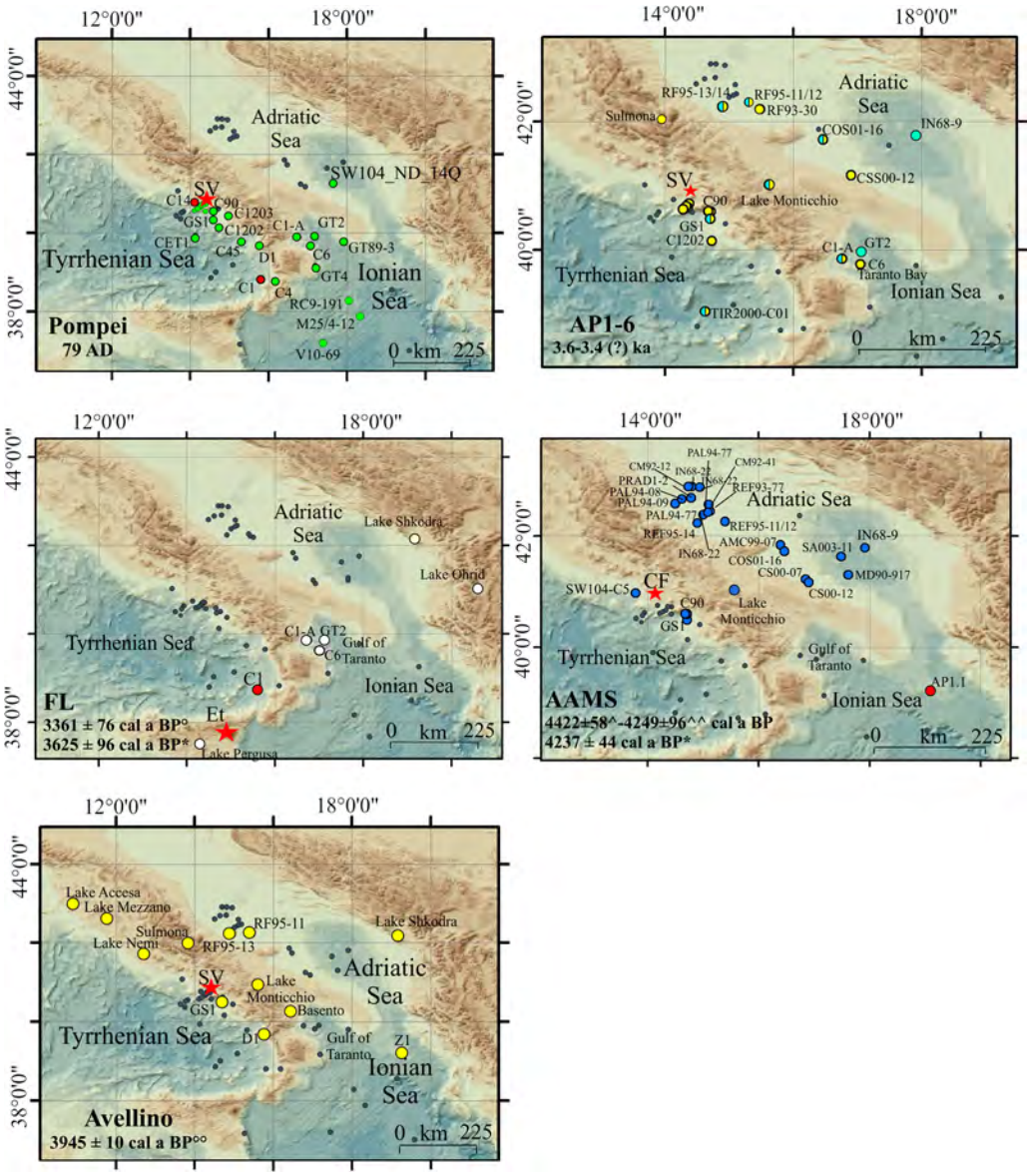

Figure 7. Occurrences of major marker tephras in the Tyrrhenian, Adriatic and Ionian seas according to the results obtained here and integrated with those of the WdB-Paleo database. A number of terrestrial sites have been also included for AP, Avellino and AAMS deposits (Crocitti *et al.*, 2018 and references therein). The two further Avellino tephra in the Ionian Sea from the WdB-Paleo in addition to the south-east and north-west occurrences reported in Sulpizio *et al.* (2008, 2014) and Crocitti *et al.* (2018) allowed us to expand the southward dispersal of these products. Gray circles: core network investigated in this work; red full circles: study sites; colored circles: occurrence of the marker tephra in the core network; red stars: source vents; *: marine age. °from Coltelli *et al.* (2000); °°from Sevink *et al.* (2011); ^ from Lirer *et al.* (2013) for Agnano Monte Spina. ^^ from Smith *et al.* (2011) for Astroni. For core references see Fig. 1. [Color figure can be viewed at wileyonlinelibrary.com] [Correction added on 13th November 2019, after first online publication: Figure 7 has been replaced with new version of Figure.]

Copyright © 2019 John Wiley & Sons, Ltd.

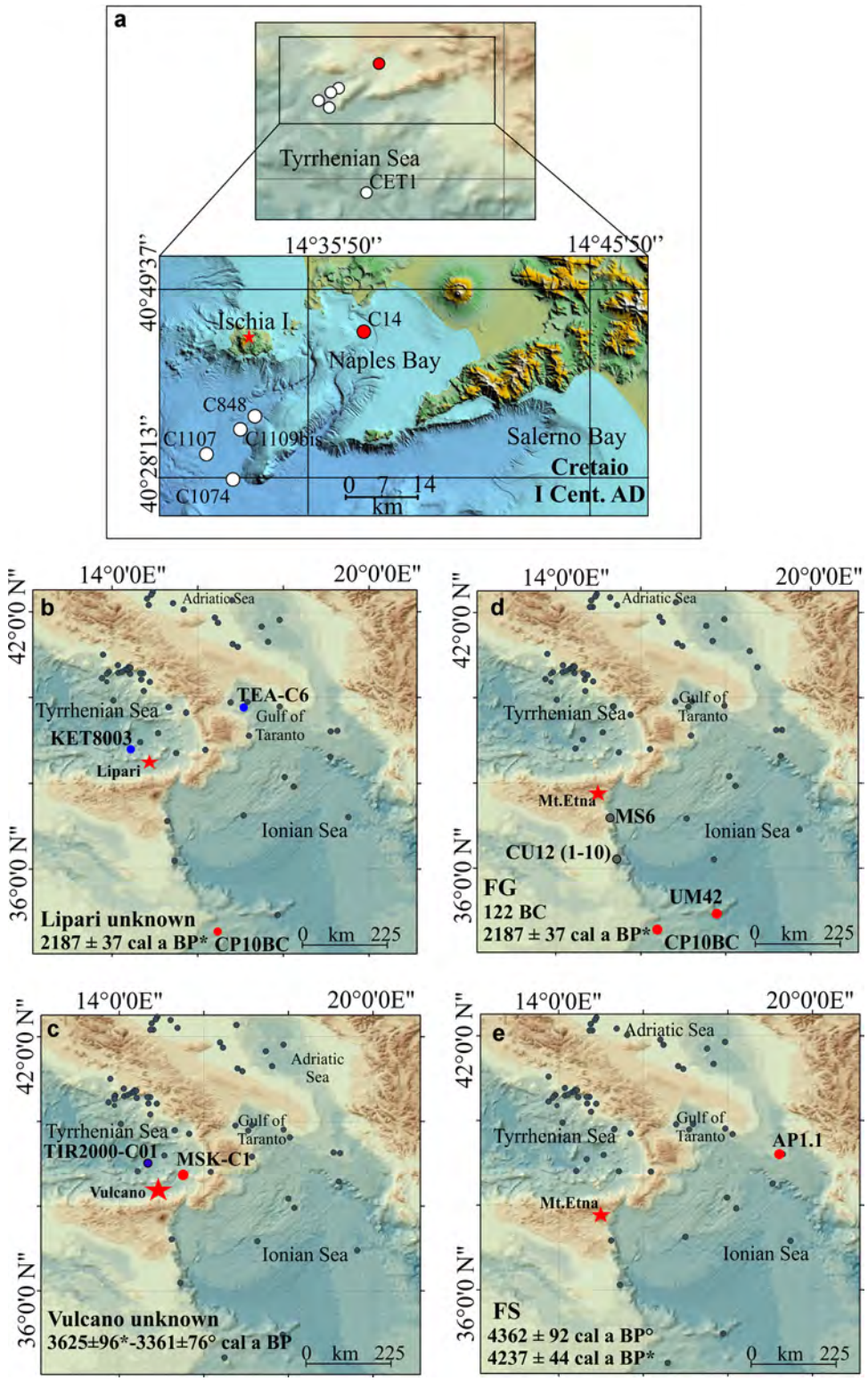

Figure 8. (a) Occurrences of Cretaio, (b,c) Lipari and Vulcano and (d,e) Mt Etna tephras and cryptotephras emplaced during the Late Holocene. For key, see Fig. 7. [Color figure can be viewed at wileyonlinelibrary.com]

events from Italian volcanoes (e.g. Sulpizio *et al.*, 2014; Crocitti *et al.*, 2018).

All the new occurrences of major 79 AD, FL and the AAMS group tephras are well within their dispersal area (Fig. 7). The recent recovery of 79 AD deposits in the southern Adriatic, in particular, extends their dispersal eastward, thus providing a key correlation marker for the three marine basins (Jalali *et al.*, 2018). Recognition of the FL tephra offshore Capo Vaticano represents its first finding in the southern Tyrrhenian. Accordingly, core C1 can be regarded as the most complete marine record where this long-lasting eruption can be observed in its distal facies. Notwithstanding the small amount of glass shards, recognition of the AAMS group at the AP1 site is also of great interest, as it allows us to extend to the south-east (i.e. towards the northern Ionian Sea) the dispersal of these products, which are recorded in many Adriatic sequences.

The new finding in the Bay of Naples of Cretaio tephra allows us to expand the distribution of this deposit towards

Copyright © 2019 John Wiley & Sons, Ltd.

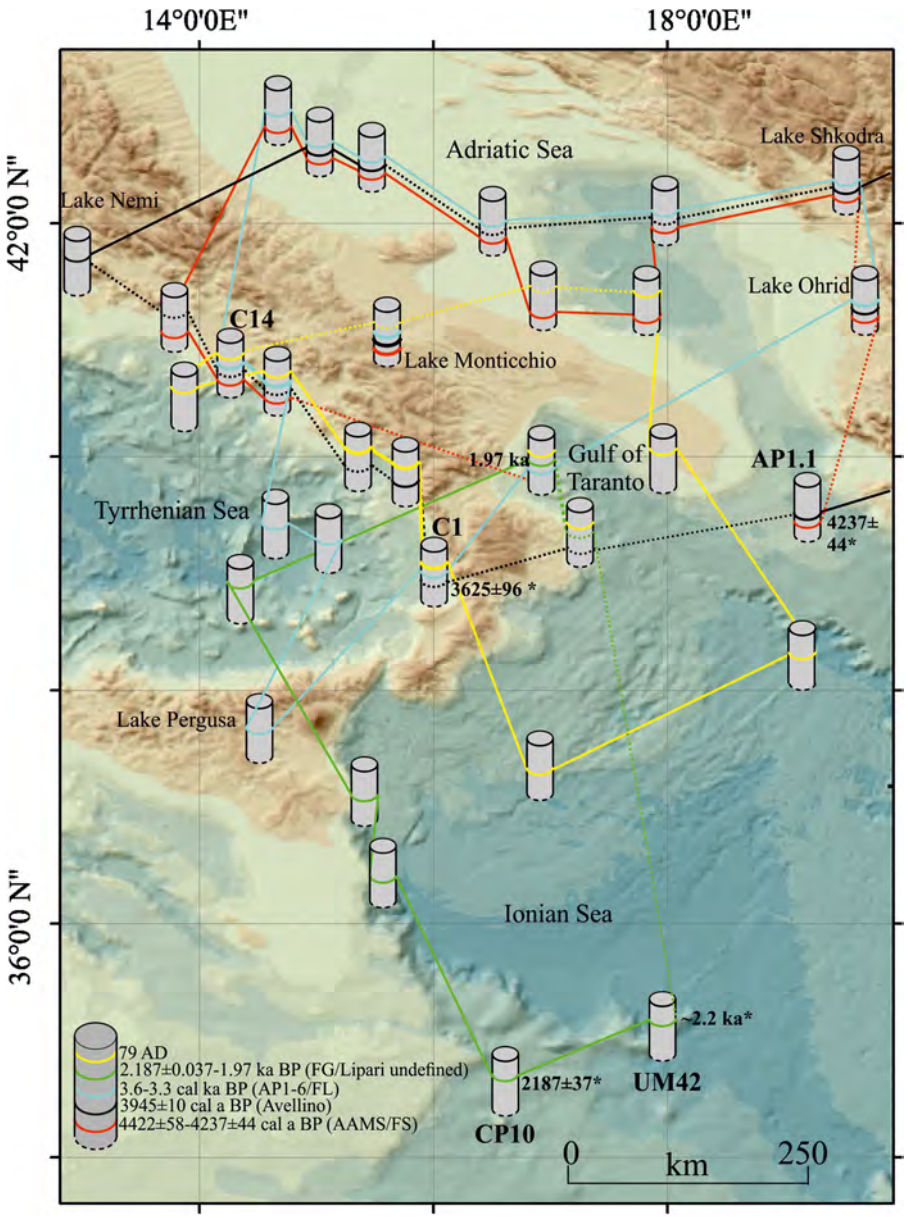

Figure 9. Sketch map of isochrons for the Central Mediterranean Sea during the 4.4 ka –79 AD time interval. Some continuous and age-constrained lacustrine sequences have been included (e.g. Lake Monticchio: Wulf *et al.*, 2004, 2008; Lake Ohrid: Caron *et al.*, 2010; Lake Shkodra: Sulpizio *et al.*, 2010; Lake Nemi: Calanchi *et al.*, 1996). The ~3.9-ka horizon corresponding to the Avellino event extends up to the Marmara Sea (Çağatay *et al.*, 2015). *Marine age from this study. Dashed lines link archives where the isochrons are inferred. [Color figure can be viewed at wileyonlinelibrary.com] [Correction added on 13th November 2019, after first online publication: Figure 9 has been replaced with new version of Figure.]

the east, a deposit that occurs significantly along the Campania margin, thus assuming a 'local' stratigraphic relevance (Fig. 8). The same can be ascribed to the uncorrelated Vulcano tephra found between the Marsili Basin and Capo Vaticano offshore. The Lipari tephra has a striking regional significance, as it occurs in all the three marine areas surrounding the Italian Peninsula and it is well age-constrained in the Taranto Bay and at the CP10 site. Finally, AP1, UM42 and CP10 represent marine records where the Late Holocene FS and FG tephras occur. These site locations agree with ash dispersal towards the east and south-east (Coltelli *et al.*, 1998, 2005), respectively. In detail, cryptotephra AP1/13 is the first occurrence in the marine setting of FS deposits, whereas UM42 and CP10 represent the more distal findings of FG tephra, which can be definitely regarded as a regional stratigraphic marker.

Isochrons

The availability of continuous isochronous markers over wide areas of the central and western Mediterranean provides a means to verify the correlation of short- and long-term climate oscillations between terrestrial and marine systems, enabling us to better understand the local–regional effects of climate change and the connections among different depositional environments (e.g. Margaritelli *et al.*, 2018). This integrated approach also represents a tool to match the possible interaction between climate changes and modifications made by human societies and their adaptive strategies during the last millennia (e.g. Büntgen *et al.*, 2011; Holmgren *et al.*, 2016 and references therein). These are issues of great relevance for the study of the 4.4–2.0 ka time interval characterized by abrupt climatic changes (e.g. the 4.2-ka event; Bini *et al.*, 2019), increasing human activities and, at the same time, recurrent explosive eruptions from different sources that produced widely dispersed tephra. Some of them, such as Agnano Monte Spina, Avellino and FL, have a relevant climatostratigraphic position in Bronze Age (ca. 4.2–2.9 cal ka BP; Zanchetta *et al.*, 2019 and references therein) archives of the central Mediterranean. In this context, our work provides a number of isochronous stratigraphic horizons that have been traced according to our new results integrated with the WdB-Paleo database for the study area (Fig. 9).

The isochron corresponding to the 79 AD event crosses southern Italy and surrounding seas and, at some sites in the southern Tyrrhenian, it locally extends to the Cretaio tephra (1st century AD). This distinctive time horizon is immediately followed by the newly reported horizon, which covers the

Copyright © 2019 John Wiley & Sons, Ltd.

2187 ± 37 cal a BP to ca. 1.97k cal a BP time interval linking archives in the southern Tyrrhenian, Gulf of Taranto and south-western Ionian. It is targeted by the Lipari tephra at all sites and by a very well expressed FG tephra in the Ionian (Figs 5, 8 and 9). The ca. 3.6–3.3 ka time interval can be traced in the whole area and targeted mostly by the AP deposits, locally also by the FL (southern Tyrrhenian and Gulf of Taranto) and the undefined tephra from Vulcano (southern Tyrrhenian). Limitations in the use of this isochron may arise, however, from the chronological ambiguities previously described, and which can be resolved only by further investigations at proximal sites and by critical revision of the data at distal sites for the AP deposits. Similar considerations can be made for the 4422 ± 58 to 4237 ± 44 cal a BP time span targeted by the AAMS group in the southern Tyrrhenian and Adriatic seas, in the Balkans and for the first time in the northern Ionian Sea where the Etnean FS tephra also occurs. Critical revision of distal tephra correlations, made according to the updated single glass database, might in fact allow us to discriminate the single event from Campi Flegrei within the AAMS group, thus providing a narrower time interval for the study area.

Concluding remarks

The results presented in this work provide new insights into the chronology and distribution of tephras and cryptotephras in the central Mediterranean during the ca. 4.4–2.0 ka time interval. The analyzed tephras comprised both markers associated with well-known, widespread Plinian events, and other deposits, characterized by narrower areal distribution or documented for the first time in the marine setting. These products have been characterized in detail, mapped and integrated with an existing database to produce a high-resolution tephrostratigraphic framework for the basin. A further outcome was the definition of five isochrons, which have the potential to correlate and synchronize paleoclimate archives. Further research developments to improve the stratigraphic framework presented in this study will probably require enhanced analysis of fine-grained cryptotephra and the resolution of chronological discrepancies for selected Late Holocene volcanic events of the central Mediterranean region.

Supporting information

Additional supporting information may be found in the online version of this article at the publisher's web-site.

Table S1. Results of the analytical routine of secondarystandards

Table S2. Selected chronological data at both proximaland distal sites

Figure S1. Photographs at the optical microscope of thestudied deposits

Acknowledgements. This work is dedicated to *Urania* R/V-CNR crews for their invaluable contribution to the marine research over the years. C. Corselli is acknowledged for many years of cooperation including *Urania* 1994 and 1998 cruises and UM42 and AP1.1 core recovery. NWO/NIOZ is acknowledged for shiptime, NIOZ-technicians and *Pelagia* crew are thanked for collaboration during the Cortado-2011 cruise. R. de Gennaro is acknowledged for his assistance during SEM-EDS acquisition and A. Filippidi for sorting out samples in Utrecht. Biagio Giaccio and an anonymous reviewer are acknowledged for their comments and suggestions that improved the quality of the manuscript. M. Gore, D. Gahan and A. Fletcher helped D.D.I. to think of this 'question of time'. Financial support for the Marisk12 cruise was provided by the Programma Operativo Nazionale (PON 2007-2013) funded by the Italian Ministry of University and Research – Project MONICA (grant PON01_01525). This research was financially supported by the Project of Strategic Interest NextData PNR 2011-2013 (www.nextdataproject.it) and by the ERC-Consolidator TIMED project (REP-683237).

Abbreviations. AAMS, Agnano Mt Spina and Astroni eruptions; AMS, accelerator mass spectrometry; AP, Avellino–Pompeii; bsf, below sea floor; bsl, below sea level; HKCA, high-K calc-alkaline; SEM-EDS, scanning electron microscopy/energy-dispersive spectrometry; SHO, shoshonitic; SR, sedimentation rate; TAS, total alkali–silica.

References

Abbott PM, Griggs AJ, Bourne AJ, *et al.* 2018. Tracing marine cryptotephras in the North Atlantic during the last glacial period: protocols for identification, characterisation and evaluating depositional controls. *Marine Geology* **401**: 81–97, https://doi.org/10.1016/j.margeo.2018.04.008

Alberico I, Giliberti I, Insinga DD, *et al.* 2017. Marine sediment cores database for the Mediterranean Basin: a tool for past climatic and environmental studies. *Open Geosciences* **9**: 221–239, https://doi.org/10.1515/geo-2017-0019

Albert PG, Tomlinson EL, Lane CS, *et al.* 2013. Late glacial explosive activity on Mount Etna: implications for proximal–distal tephra correlations and the synchronisation of Mediterranean archives. *Journal of Volcanology and Geothermal Research* **265**: 9–26, https://doi.org/10.1016/j.jvolgeores.2013.07.010

Albert PG, Tomlinson EL, Smith VC, *et al.* 2012. Marine–continental tephra correlations: volcanic glass geochemistry from the Marsili Basin and the Aeolian Islands, southern Tyrrhenian Sea, Italy. *Journal of Volcanology and Geothermal Research* **229–230**: 74–94, https://doi.org/10.1016/j.jvolgeores.2012.03.009

Albert PG, Tomlinson EL, Smith VC, *et al.* 2017. Glass geochemistry of pyroclastic deposits from the Aeolian Islands in the last 50 ka: a proximal database for tephrochronology. *Journal of Volcanology and Geothermal Research* **336**: 81–107, https://doi.org/10.1016/j.jvolgeores.2017.02.008

Bini M, Zanchetta G, Perşoiu A, *et al.* 2019. The 4.2 ka BP Event in the Mediterranean region: an overview. *Climate of the Past* **15**: 555–577, https://doi.org/10.5194/cp-15-555-2019

Bronk Ramsey C. 2008. Deposition models for chronological records. *Quaternary Science Reviews* **27**: 42–60, https://doi.org/10.1016/j.quascirev.2007.01.019

Bronk Ramsey C. 2009. Bayesian analysis of radiocarbon dates. *Radiocarbon* **51**: 337–360, https://doi.org/10.1017/S0033822200033865

Bronk Ramsey C, Albert PG, Blockley SPE, *et al.* 2015. Improved age estimates for key Late Quaternary European tephra horizons in the RESET lattice. *Quaternary Science Reviews* **118**: 18–32, https://doi.org/10.1016/j.quascirev.2014.11.007

Budillon F, Senatore MR, Insinga DD, *et al.* 2012. Late Holocene sedimentary changes in shallow water settings: the case of the Sele River offshore in the Salerno Gulf (south-eastern Tyrrhenian Sea, Italy). *Rendiconti Lincei* **23**: 25–43, https://doi.org/10.1007/s12210-012-0164-6

Büntgen U, Tegel W, Nicolussi K, *et al.* 2011. 2500 years of European climate variability and human susceptibility. *Science* **331**: 578–582, https://doi.org/10.1126/science.1197175, PubMed: 21233349.

Çağatay MN, Wulf S, Sancar Ü, *et al.* 2015. The tephra record from the Sea of Marmara for the last ca. 70 ka and its palaeoceanographic implications. *Marine Geology* **361**: 96–110, https://doi.org/10.1016/j.margeo.2015.01.005

Calanchi N, Cattaneo A, Dinelli E, *et al.* 1998. Tephra layers in Late Quaternary sediments of the central Adriatic Sea. *Marine Geology* **149**: 191–209, https://doi.org/10.1016/S0025-3227(98)00030-9

Calanchi N, Dinelli E. 2008. Tephrostratigraphy of the last 170 ka in sedimentary successions from the Adriatic Sea. *Journal of Volcanology and Geothermal Research* **177**: 81–95, https://doi.org/10.1016/j.jvolgeores.2008.06.008

Calanchi N, Dinelli E, Lucchini F, *et al.* 1996. Chemostratigraphy of late Quaternary sediments from Lake Albano and central Adriatic Sea cores (PALICLAS Project). *Memorie-Istituto Italiano di Idrobiologia* **55**: 247–263.

Caron B, Sulpizio R, Zanchetta G, *et al.* 2010. The Late Holocene to Pleistocene tephrostratigraphic record of Lake Ohrid (Albania).

Copyright © 2019 John Wiley & Sons, Ltd.

Comptes Rendus Geoscience **342**: 453–466, https://doi.org/10.1016/j.crte.2010.03.007

Cini Castagnoli GC, Bonino G, Caprioglio F, *et al.* 1990. The carbonate profile of two recent Ionian Sea cores: evidence that the sedimentation rate is constant over the last millennia. *Geophysical Research Letters* **17**: 1937–1940, https://doi.org/10.1029/GL017i011p01937

Coltelli M, Del Carlo P, Vezzoli L. 1998. Discovery of a Plinian basaltic eruption of Roman age at Etna volcano, Italy. *Geology* **26**: 1095–1098, https://doi.org/10.1130/0091-7613(1998)026, <1095:DOAPBE>2.3.CO;2].

Coltelli M, Del Carlo P, Pompilio M, *et al.* 2005. Explosive eruption of a picrite: the 3930 BP subplinian eruption of Etna volcano (Italy). *Geophysical Research Letters* **32**: L23307, https://doi.org/10.1029/2005GL024271

Coltelli M, Del Carlo P, Vezzoli L. 2000. Stratigraphic constraints for explosive activity in the past 100 ka at Etna Volcano, Italy. *International Journal of Earth Sciences* **89**: 665–677, https://doi.org/10.1007/s005310000117

Conticelli S, Laurenzi MA, Giordano G, *et al.* 2010. Leucite-bearing (kamafugitic/leucititic) and -free (lamproitic) ultrapotassic rocks and associated shoshonites from Italy: constraints on petrogenesis and geodynamics. *Journal of the Virtual Explorer*, https://doi.org/10.3809/jvirtex.2010.00251, 36: paper 20.

Cosentino C, Molisso F, Scopelliti G, *et al.* 2017. Benthic foraminifera as indicators of relative sea-level fluctuations: paleoenvironmental and paleoclimatic reconstruction of a Holocene marine succession (Calabria, south-eastern Tyrrhenian Sea). *Quatenary International* **439**: 79–101.

Crocitti M, Sulpizio R, Insinga DD, *et al.* 2018. On ash dispersal from moderately explosive volcanic eruptions: examples from Holocene and Late Pleistocene eruptions of Italian volcanoes. *Journal of Volcanology and Geothermal Research*, https://doi.org/10.1016/j.jvolgeores.2018.07.009

D'Antonio M, Mariconte R, Arienzo I, *et al.* 2016. Combined Sr–Nd isotopic and geochemical fingerprinting as a tool for identifying tephra layers: application to deep-sea cores from eastern Mediterranean Sea. *Chemical Geology* **443**: 121–136, https://doi.org/10.1016/j.chemgeo.2016.09.022

De Alteriis G, Insinga DD, Morabito S, *et al.* 2010. Age of submarine debris avalanches and tephrostratigraphy offshore Ischia Island, Tyrrhenian Sea, Italy. *Marine Geology* **278**: 1–18, https://doi.org/10.1016/j.margeo.2010.08.004

De Martini PM, Barbano MS, Smedile A, *et al.* 2010. A 4000 yrs long record of tsunami deposits along the coast of the Augusta Bay (eastern Sicily, Italy): paleoseismological implications. *Marine Geology* **276**: 42–57 , https://doi.org/10.1016/j.margeo.2010.07.005

Di Donato V, Insinga DD, Iorio M, *et al.* 2019. The palaeoclimatic and palaeoceanographic history of the Gulf of Taranto (Mediterranean Sea) in the last 15 ky. *Global and Planetary Change* **172**: 278–297, https://doi.org/10.1016/j.gloplacha.2018.10.014

Di Roberto A, Rosi M, Bertagnini A, *et al.* 2008. Deep water gravity core from the Marsili Basin (Tyrrhenian Sea) records Pleistocenic-Holocenic explosive events and instability of the Aeolian Archipelago, (Italy). *Journal of Volcanology and Geothermal Research* **177**: 133–144, https://doi.org/10.1016/j.jvolgeores.2008.01.009

Forni F, Lucchi F, Peccerillo A, *et al.* 2013. Stratigraphic and geological evolution of the Lipari volcanic complex (central Aeolian archipelago. In *The Aeolian Islands Volcanoes*, Lucchi F, Peccerillo A, Keller J, Tranne CA, Rossi PL (eds). Geological Society: London, Memoirs; 213–279.

Freydier R, Michard A, De Lange G, *et al.* 2001. Nd isotopic compositions of eastern Mediterranean sediments: tracers of the Nile influence during sapropel S1 formation? *Marine Geology* **177**: 45–62, https://doi.org/10.1016/S0025-3227(01)00123-2

Geraga M, Mylona G, Tsaila-Monopoli ST, *et al.* 2008. Northeastern Ionian Sea: palaeoceanographic variability over the last 22 ka. *Journal of Marine Systems* **74**: 623–638, https://doi.org/10.1016/j.jmarsys.2008.05.019

Giaccio B, Niespolo EM, Pereira A, *et al.* 2017. First integrated tephrochronological record for the last ~190 kyr from the Fucino Quaternary lacustrine succession, central Italy. *Quaternary Science Reviews* **158**: 211–234, https://doi.org/10.1016/j.quascirev.2017.01.004

Goslar T, Czernik J, Goslar E. 2004. Low-energy 14C AMS in Poznań Radiocarbon Laboratory, Poland. *Nuclear Instruments and Methods in Physics Research Section B* **223–224**: 5–11, https://doi.org/10.1016/j.nimb.2004.04.005

Holmgren K, Gogou A, Izdebski A, *et al.* 2016. Mediterranean Holocene climate, environment and human societies. *Quaternary Science Reviews* **136**: 1–4, https://doi.org/10.1016/j.quascirev.2015.12.014

Insinga D, Molisso F, Lubritto C, *et al.* 2008. The proximal marine record of Somma–Vesuvius volcanic activity in the Naples and Salerno bays, Eastern Tyrrhenian Sea, during the last 3 kyrs. *Journal of Volcanology and Geothermal Research* **177**: 170–186, https://doi.org/10.1016/j.jvolgeores.2007.07.011

Insinga DD, Tamburrino S, Lirer F, *et al.* 2014. Tephrochronology of the astronomically-tuned KC01B deep-sea core, Ionian Sea: insights into the explosive activity of the Central Mediterranean area during the last 200 ka. *Quaternary Science Reviews* **85**: 63–84, https://doi.org/10.1016/j.quascirev.2013.11.019

Iorio M, Liddicoat J, Budillon F, *et al.* 2009. Palaeomagnetic secular variation time constraint on Late Neogene geological events in slope sediment from the eastern Tyrrhenian Sea. *SEPM Special Publications* **92**: 233–246.

Jalali B, Sicre MA, Klein V, *et al.* 2018. Deltaic and coastal sediments as recorders of Mediterranean regional climate and human impact over the past three millennia. *Paleoceanography and Paleoclimatology* **33**: 579–593, https://doi.org/10.1029/2017PA003298

Keller J, Ryan WBF, Ninkovich D, *et al.* 1978. Explosive volcanic activity in the Mediterranean over the past 200,000 yr as recorded in deep-sea sediments. *Geological Society of America Bulletin* **89**: 591–604, https://doi.org/10.1130/0016-7606(1978)89, <591:EVAITM>2.0.CO;2].

Kuehn SC, Froese DG, Shane PAR. 2011. The INTAV intercomparison of electron-beammicroanalysis of glass by tephrochronology laboratories: results and recommendations. *Quaternary International* **246**: 19–47, https://doi.org/10.1016/j.quaint.2011.08.022

Le Maitre RW. 2005. Igneous rocks. A classification and glossary of terms. Recommendations of the International Union of Geological Sciences, *Subcommission on the Systematics of Igneous Rocks*. Cambridge University Press: Cambridge.

Lirer F, Sprovieri M, Ferraro L, *et al.* 2013. Integrated stratigraphy for the Late Quaternary in the eastern Tyrrhenian Sea. *Quaternary International* **292**: 71–85, https://doi.org/10.1016/j.quaint.2012.08.2055

Lowe JJ, Blockley S, Trincardi F, *et al.* 2007. Age modelling of late Quaternary marine sequences in the Adriatic: towards improved precision and accuracy using volcanic event stratigraphy. *Continental Shelf Research* **27**: 560–582, https://doi.org/10.1016/j.csr.2005.12.017

Lubritto C, Ricci P, Germinario C, *et al.* 2018. Radiocarbon dating of mortars: contamination effects and sample characterisation. The case-study of Andalusian medieval castles (Jaén, Spain). *Measurement: Journal of the International Measurement Confederation* **118**: 362–371.

Lucchi F, Tranne CA, De Astis G, *et al.* 2008. Stratigraphy and significance of Brown Tuffs on the Aeolian Islands (southern Italy). *Journal of Volcanology and Geothermal Research* **177**: 49–70, https://doi.org/10.1016/j.jvolgeores.2007.11.006

Margaritelli G, Cisneros M, Cacho I, *et al.* 2018. Climatic variability over the last 3000 years in the central – western Mediterranean Sea (Menorca Basin) detected by planktonic foraminifera and stable isotope records. *Global and Planetary Change* **169**: 179–187, https://doi.org/10.1016/j.gloplacha.2018.07.012

Margaritelli G, Vallefuoco M, Di Rita F, *et al.* 2016. Marine response to climate changes during the last five millennia in the central Mediterranean Sea. *Global and Planetary Change* **142**: 53–72.

Matthews IP, Trincardi F, Lowe JJ, *et al.* 2015. Developing a robust tephrochronological framework for Late Quaternary marine records in the southern Adriatic Sea: new data from core station SA03-11. *Quaternary Science Reviews* **118**: 84–104, https://doi.org/10.1016/j.quascirev.2014.10.009

Micallef A, Georgiopoulou A, Mountjoy J, *et al.* 2016. Outer shelf seafloor geomorphology along a carbonate escarpment: the eastern Malta Plateau, Mediterranean Sea. *Continental Shelf Research* **131**: 12–27, https://doi.org/10.1016/j.csr.2016.11.002

Morabito S, Petrosino P, Milia A, *et al.* 2014. A multidisciplinary approach for reconstructing the stratigraphic framework of the last 40ka in a bathyal area of the eastern Tyrrhenian Sea. *Global and Planetary Change* **123**: 121–138, https://doi.org/10.1016/j.gloplacha.2014.10.005

Copyright © 2019 John Wiley & Sons, Ltd.

Munno R, Petrosino P. 2004. New constraints on the occurrence of Y-3 Upper Pleistocene tephra marker layer in the Tyrrhenian Sea. *Quaternario* **17**: 11–20.

Munno R, Petrosino P. 2007. The late Quaternary tephrostratigraphical record of the San Gregorio Magno basin (southern Italy). *Journal of Quaternary Science* **22**: 247–266, https://doi.org/10.1002/jqs.1025

Orsi G, Gallo G, Heiken G, *et al.* 1992. A comprehensive study of pumice formation and dispersal: the Cretaio tephra of Ischia (Italy). *Journal of Volcanology and Geothermal Research* **53**: 329–354, https://doi.org/10.1016/0377-0273(92)90090-Z

Paterne M, Guichard F, Duplessy JC, *et al.* 2008. A 90,000–200,000 yrs marine tephra record of Italian volcanic activity in the Central Mediterranean Sea. *Journal of Volcanology and Geothermal Research* **177**: 187–196, https://doi.org/10.1016/j.jvolgeores.2007.11.028

Paterne M, Guichard F, Labeyrie J. 1988. Explosive activity of the South Italian volcanoes during the past 80,000 years as determined by marine tephrochronology. *Journal of Volcanology and Geothermal Research* **34**: 153–172, https://doi.org/10.1016/0377-0273(88)90030-3

Pearce NJG, Westgate JA, Perkins WT, *et al.* 1999. The application of laser ablation ICP-MS to the analysis of volcanic glass shards from tephra deposits: bulk glass and single shard analysis. *Global and Planetary Change* **21**: 151–171, https://doi.org/10.1016/S0921-8181(99)00012-0

Peccerillo A. 2005. Petrogenesis and Geodynamics in Italy, *Plio-Quaternary Magmatism in Italy Petrology, Geochemistry, Geodynamics*. Springer: Heidelberg.

Pepe F, Di Donato V, Insinga D, *et al.* 2018. Seismic stratigraphy of upper Quaternary shallow-water contourite drifts in the Gulf of Taranto (Ionian Sea, southern Italy). *Marine Geology* **397**: 79–92, https://doi.org/10.1016/j.margeo.2017.12.004

Petrosino P, Insinga DD, Molisso F, *et al.* 2018. Tephra markers for the timing of morphotectonic phases in the Campi Flegrei caldera Crossing New Frontiers INTAV International Field Conference on Tephrochronology 'Tephra Hunt in Transylvania' Moieciu de Sus, Romania. 24 June - 1 July 2018

Reimer PJ, Bard E, Bayliss A, *et al.* 2013. IntCal13 and Marine13 radiocarbon age calibration curves 0–50,000 years cal BP. *Radiocarbon* **55**: 1869–1887.

Sacchi M, Insinga D, Milia A, *et al.* 2005. Stratigraphic signature of the Vesuvius 79 AD event off the Sarno prodelta system, Naples Bay. *Marine Geology* **222–223**: 443–469, https://doi.org/10.1016/j.margeo.2005.06.014

Sacchi M, Molisso F, Violante C, *et al.* 2009. Insights into flood-dominated fan-deltas: very high-resolution seismic examples off the Amalfi cliffed coasts, eastern Tyrrhenian Sea. Geological Society, London, Special Publications 322: 33–71, https://doi.org/10.1144/SP322.2

Sacchi M, Pepe F, Corradino M, *et al.* 2014. The Neapolitan Yellow Tuff caldera offshore the Campi Flegrei: stratal architecture and kinematic reconstruction during the last 15 ky. *Marine Geology* **354**: 15–33, https://doi.org/10.1016/j.margeo.2014.04.012

Sadori L, Narcisi B. 2001. The postglacial record of environmental history from Lago di Pergusa, Sicily. *Holocene* **11**: 655–671, https://doi.org/10.1191/09596830195681

Sadori L, Ortu E, Peyron O, *et al.* 2013. The last 7 millennia of vegetation and climate changes at Lago di Pergusa (central Sicily, Italy). *Climate of the Past* **9**: 1969–1984, https://doi.org/10.5194/cp-9-1969-2013

Santacroce R, Cioni R, Marianelli P, *et al.* 2008. Age and whole rock–glass compositions of proximal pyroclastics from the major explosive eruptions of Somma-Vesuvius: a review as a tool for distal tephrostratigraphy. *Journal of Volcanology and Geothermal Research* **177**: 1–18, https://doi.org/10.1016/j.jvolgeores.2008.06.009

Sevink J, van Bergen MJ, van der Plicht J, *et al.* 2011. Robust date for the Bronze Age Avellino eruption (Somma-Vesuvius): 3945 ± 10 cal BP (1995 ± 10 cal BC). *Quaternary Science Reviews* **30**: 1035–1046, https://doi.org/10.1016/j.quascirev.2011.02.001

Siani G, Paterne M, Arnold M, *et al.* 2000. Radiocarbon reservoir ages in the Mediterranean Sea and Black Sea. *Radiocarbon* **42**: 271–280, https://doi.org/10.1017/S0033822200059075

Siani G, Sulpizio R, Paterne M, *et al.* 2004. Tephrostratigraphy study for the last 18,000 C years in a deep-sea sediment sequence for the South Adriatic. *Quaternary Science Reviews* **23**: 2485–2500, https://doi.org/10.1016/j.quascirev.2004.06.004

Sigurdsson H, Carey S, Cornell W, *et al.* 1985. The eruption of Vesuvius in A.D. 79. *National Geographic Research* **1**: 332–387.

Smedile A, De Martini PM, Pantosti D, *et al.* 2011. Possible tsunami signatures from an integrated study in the Augusta Bay offshore (Eastern Sicily—Italy). *Marine Geology* **281**: 1–13, https://doi.org/10.1016/j.margeo.2011.01.002

Smith VC, Isaia R, Pearce NJG. 2011. Tephrostratigraphy and glass compositions of post-15 kyr Campi Flegrei eruptions: implications for eruption history and chronostratigraphic markers. *Quaternary Science Reviews* **30**: 3638–3660, https://doi.org/10.1016/j.quascirev.2011.07.012

Sulpizio R, Bonasia R, Dellino P, *et al.* 2008. Discriminating the long distance dispersal of fine ash from sustained columns or near ground ash clouds: the example of the Pomici di Avellino eruption (Somma-Vesuvius, Italy). *Journal of Volcanology and Geothermal Research* **177**: 263–276, https://doi.org/10.1016/j.jvolgeores.2007.11.012

Sulpizio R, Van Welden A, Caron B, *et al.* 2010. The Holocene tephrostratigraphic record of Lake Shkodra (Albania and Montenegro). *Journal of Quaternary Science* **25**: 633–650, https://doi.org/10.1002/jqs.1334

Sulpizio R, Zanchetta G, Caron B, *et al.* 2014. Volcanic ash hazard in the Central Mediterranean assessed from geological data. *Bulletin of Volcanology* **76**: 866–873, https://doi.org/10.1007/s00445-014-0866-y

Tomlinson EL, Arienzo I, Civetta L, *et al*. 2012. Geochemistry of the Phlegraean Fields (Italy) proximal sources for major Mediterranean tephras: implications for the dispersal of Plinian and co-ignimbritic components of explosive eruptions. *Geochimica et Cosmochimica Acta* **93**: 102–128, https://doi.org/10.1016/j.gca.2012.05.043

Tomlinson EL, Smith VC, Albert PG, *et al.* 2015. The major and trace element glass compositions of the productive Mediterranean volcanic sources: tools for correlating distal tephra layers in and around Europe. *Quatenary Science Reviews* **118**: 48–66.

Van Der Borg K, Alderliesten C, De Jong AFM, *et al.* 1997. Precision and mass fractionation in 14C analysis with AMS. *Nuclear Instruments and Methods in Physics Research Section B* **123**: 97–101, https://doi.org/10.1016/S0168-583x(96)00713-6

Vogel H, Zanchetta G, Sulpizio R, *et al.* 2010. A tephrostratigraphic record for the last glacial–interglacial cycle from Lake Ohrid, Albania and Macedonia. *Journal of Quaternary Science* **25**: 320–338, https://doi.org/10.1002/jqs.1311

Voltaggio M, Branca M, Tuccimei P, *et al.* 1995. Leaching procedure used in dating young potassic volcanic rocks by the 226Ra/230Th method. *Earth and Planetary Science Letters* **136**: 123–131, https://doi.org/10.1016/0012-821x(95)00177-E

Wu J, Böning P, Pahnke K, *et al.* 2016. Unraveling North-African riverine and eolian contributions to central Mediterranean sediments during Holocene sapropel S1 formation. *Quaternary Science Reviews* **152**: 31–48, https://doi.org/10.1016/j.quascirev.2016.09.029

Wu J, Liu Z, Stuut JW, *et al.* 2017. North-African paleodrainage discharges to the central Mediterranean during the last 18,000 years: a multiproxy characterization. *Quaternary Science Reviews* **163**: 95–113, https://doi.org/10.1016/j.quascirev.2017.03.015

Wulf S, Kraml M, Brauer A, *et al.* 2004. Tephrochronology of the 100ka lacustrine sediment record of Lago Grande di Monticchio (southern Italy). *Quaternary International* **122**: 7–30, https://doi.org/10.1016/j.quaint.2004.01.028

Wulf S, Kraml M, Keller J. 2008. Towards a detailed distal tephrostratigraphy in the central Mediterranean: the last 20,000 yrs record of Lago Grande di Monticchio. *Journal of Volcanology and Geothermal Research* **177**: 118–132, https://doi.org/10.1016/j.jvolgeores.2007.10.009

Zanchetta G, Bini M, Di Vito MA, *et al.* 2019. Tephrostratigraphy of paleoclimatic archives in central Mediterranean during the Bronze Age. *Quaternary International* **499**: 186–194, https://doi.org/10.1016/j.quaint.2018.06.012

Zanchetta G, Sulpizio R, Roberts N, *et al.* 2011. Tephrostratigraphy, chronology and climatic events of the Mediterranean basin during the Holocene: an overview. *The Holocene* **21**: 33–52, https://doi.org/10.1177/0959683610377531

Copyright © 2019 John Wiley & Sons, Ltd.